Deterministic splicing of *Dscam2* is regulated by Muscleblind

Joshua Shing Shun Li and S. Sean Millard

School of Biomedical Sciences, The University of Queensland, Brisbane, 4072, Australia

Correspondence: s.millard@uq.edu.au

Summary

Alternative splicing of genes increases the number of distinct proteins in a cell. In the brain it is highly prevalent, presumably because proteome diversity is crucial for establishing the complex circuitry between trillions of neurons. To provide individual cells with different repertoires of protein isoforms, however, this process must be regulated. Previously, we found that the mutually exclusive alternative splicing of a cell surface protein, *Dscam2* produces two isoforms (exon 10A and 10B) with unique binding properties. This splicing event is tightly regulated and crucial for maintaining axon terminal size, dendritic morphology and synaptic numbers. Here, we show that *Drosophila* Muscleblind (Mbl), a conserved splicing factor implicated in myotonic dystrophy, controls *Dscam2* alternative splicing. Removing *mbl* from cells that normally express isoform B induces the expression of isoform A and eliminates the expression of B, demonstrating that Mbl represses one alternative exon and selects the other. *Mbl* mutants exhibit phenotypes that are also observed in flies engineered to express a single isoform. Consistent with these observations, *mbl* expression is cell-type-specific and correlates with the expression of isoform B. Our study demonstrates how the regulated expression of a splicing factor is sufficient to provide neurons with unique protein isoforms crucial for development.

26

27

28 **Introduction**

29 Alternative splicing occurs in approximately 95% of human genes and generates
30 proteome diversity much needed for brain wiring (Pan et al., 2008; Wang et al.,
31 2008). Specifying neuronal connections through alternative splicing would require
32 regulated expression of isoforms with unique functions in different cell types to carry
33 out distinct processes. Although there are some examples of neuronal cell-type-
34 specific isoform expression (Bell et al., 2004; Iijima et al., 2014; Lah et al., 2014;
35 Norris et al., 2014; Schreiner et al., 2014; Tomioka et al., 2016), the mechanisms
36 underlying these deterministic splicing events and their functional consequences
37 remain understudied. This is due, in part, to the technical difficulties of assessing and
38 manipulating isoform expression *in vivo*, and at the single cell level. Another obstacle
39 is that most splicing regulators are proposed to be ubiquitously expressed (Nilsen and
40 Graveley, 2010). For example, the broadly expressed SR and heterogeneous nuclear
41 ribonucleoproteins (hnRNPs) typically have opposing activities, and the prevalence of
42 splice site usage is thought to be controlled by their relative abundances within the
43 cell (Blanchette et al., 2009). Although there are many examples where splicing
44 regulators are expressed in a tissue-specific manner (Calarco et al., 2009; Kuroyanagi
45 et al., 2006; Markovtsov et al., 2000; Ohno et al., 2008; Underwood et al., 2005;
46 Warzecha et al., 2009), until recently, reports of cell-type specific expression have
47 been less frequent (McKee et al., 2005; Wang et al., 2018).

48

49 In insects, Dscam2 is a cell recognition molecule that mediates self- and cell-type-
50 specific avoidance (tiling) (Funada et al., 2007; Millard et al., 2007; Millard et al.,

2010). Mutually exclusive alternative splicing of exon 10A or 10B produces two isoforms with biochemically unique extracellular domains that are regulated both spatially and temporally (Funada et al., 2007; Millard et al., 2007). Previously, we demonstrated that cell-type-specific alternative splicing of *Drosophila Dscam2* is crucial for the proper development of axon terminal size, dendrite morphology and synaptic numbers in the fly visual system (Kerwin et al., 2018; Lah et al., 2014; Li et al., 2015). Although these studies showed that disrupting cell-specific *Dscam2* alternative splicing has functional consequences, what regulates this process remained unclear. Here, we conducted an RNAi screen and identified *muscleblind* (*mbl*) as a regulator of *Dscam2* alternative splicing. Loss-of-function (LOF) and overexpression (OE) studies suggest that Mbl acts both as a splicing repressor of *Dscam2* exon 10A and as an activator of exon 10B (hereafter *Dscam2.10A* and *Dscam2.10B*). Consistent with this finding, *mbl* expression is cell-type-specific and correlates with the expression of *Dscam2.10B*. Hypomorphic *mbl* mutants exhibit visual system phenotypes that are similar to those observed in flies engineered to express one isoform in all *Dscam2*-positive cells (single isoform strains). Similarly, driving *mbl* in mushroom body neurons that normally select isoform A, induces the expression of isoform B and generates a single isoform phenotype. Although the *mbl* gene is itself alternatively spliced, we found that selection of *Dscam2.10B* does not require a specific Mbl isoform and that human MBNL1 can also regulate *Dscam2* alternative splicing. Our study provides compelling genetic evidence that the regulated expression of a highly conserved RNA binding protein, Mbl, is sufficient for the selection of *Dscam2.10B* and that disrupting this mechanism for cell-specific protein expression leads to developmental defects in neurons.

77 **Results**

78 **An RNAi screen identifies *mbl* as a repressor of *Dscam2* exon 10A selection**

79 We reasoned that the neuronal cell-type-specific alternative splicing of *Dscam2* is
80 likely regulated by RNA binding proteins, and that we could identify these regulators
81 by knocking them down in a genetic background containing an isoform reporter. In
82 photoreceptors (R cells) of third instar larvae, *Dscam2.10B* is selected whereas the
83 splicing of *Dscam2.10A* is repressed (Lah et al., 2014; Tadros et al., 2016). Given that
84 quantifying a reduction in *Dscam2.10B* isoform reporter levels is challenging
85 compared to detecting the appearance of *Dscam2.10A* in cells where it is not normally
86 expressed, we performed a screen for repressors of isoform A in R cells.

87

88 To knock down RNA binding proteins, the *glass* multimer reporter (*GMR)-GAL4* was
89 used to drive RNAi transgenes selectively in R cells. Our genetic background
90 included *UAS-Dcr-2* to increase RNAi efficiency (Dietzl et al., 2007) and *GMR-GFP*
91 to mark the photoreceptors independent of the *Gal4/UAS* system (Brand and
92 Perrimon, 1993). Lastly, a *Dscam2.10A-LexA* reporter driving *LexAOp*-myristolated
93 tdTomato (hereafter *Dscam2.10A>tdTom*; Fig. 1A) was used to visualize isoform A
94 expression (Lai and Lee, 2006; Tadros et al., 2016). As expected,
95 *Dscam2.10B>tdTom* was detected in R cell projections in the lamina plexus as well as
96 in their cell bodies in the eye-disc, whereas *Dscam2.10A>tdTom* was not (Fig. 1C-
97 1D). Overexpression of Dcr-2 in R cells did not perturb the repression of
98 *Dscam2.10A* (Fig 1O). We knocked down ~160 genes using ~250 RNAi lines (Fig 1B
99 and Table S1) and identified two independent RNAi lines targeting *mbl* that caused
100 aberrant expression of *Dscam2.10A* in R cells where it is normally absent (Fig 1F,

101 1O). The penetrance increased when animals were reared at a more optimal Gal4
102 temperature of 29°C (Mondal et al., 2007; Ni et al., 2008) (Fig 1O).
103
104 Mbl-family proteins possess evolutionarily conserved tandem CCCH zinc-finger
105 domains through which they bind pre-mRNA. Vertebrate Mbl family members are
106 involved in tissue-specific splicing and have been implicated in myotonic dystrophy
107 (Pascual et al., 2006). Formerly known as *mindmelt*, *Drosophila mbl* was first
108 identified in a second chromosome *P*-element genetic screen for embryonic defects in
109 the peripheral nervous system (Kania et al., 1995). *Mbl* produces multiple isoforms
110 through alternative splicing (Begemann et al., 1997; Irion, 2012), and its function has
111 been most extensively characterized in fly muscles where both hypomorphic
112 mutations and sequestration of the protein by repeated CUG sequences within an
113 mRNA lead to muscle defects (Artero et al., 1998; Llamusi et al., 2013). To validate
114 the RNAi phenotype, we tested *Dscam2.10A>tdTom* expression in *mbl* loss-of-
115 function (LOF) mutants. Since *mbl* LOF results in lethality, we first conducted
116 complementation tests on six *mbl* mutant alleles to identify viable hypomorphic
117 combinations. These included two alleles created previously via imprecise *P*-element
118 excision (mbl^{e127} and mbl^{e27}; Begemann et al. 1997) two MiMIC splicing traps
119 ($mbl^{MI00976}$ and $mbl^{MI04093}$; (Venken et al., 2011) and two 2nd chromosome deficiencies
120 (*Df(2R)BSC154* and *Df(2R)Exel6066*; Fig 1F-1G). Consistent with previous reports,
121 the complementation tests confirmed that the majority of the alleles were lethal over
122 one another (Fig 1G) (Kania et al., 1995). However, we identified two *mbl*
123 transheterozygous combinations that were partially viable and crossed these into a
124 *Dscam2.10A>tdTom* reporter background. Both $mbl^{e127}/mbl^{MI00976}$ and
125 $mbl^{MI04093}/mbl^{MI00976}$ animals presented aberrant *Dscam2.10A* expression in R cells

126 when compared to heterozygous and wild-type controls (Fig 1H-O). *Mbl* mutant
127 mosaic clones also exhibited aberrant *Dscam2.10A>tdTom* expression in R cells (Fig
128 S1A-S1F). The weakest allele, mbl^{M00976}, which removes only a proportion of the *mbl*
129 isoforms, was the only exception (Fig S1E-S1F).
130
131 One alternative explanation of how *Dscam2.10A>tdTom* expression could get
132 switched-on in *mbl* mutants, is through exon 10 skipping. Removing both alternative
133 exons simultaneously does not result in a frameshift mutation, and since the Gal4 in
134 our reporters is inserted directly downstream of the variable exons (in exon 11), it
135 would still be expressed. To test this possibility, we amplified *Dscam2* sequences
136 between exon 9 and 11 in $mbl^{e127}/mbl^{MI00976}$ transheterozygous animals using RT-PCR.
137 In both control and *mbl* LOF mutants, we detected RT-PCR products (~690bp) that
138 corresponded to the inclusion of exon 10 (A or B) and failed to detect products
139 (~390bp) that would result from exon 10 skipping (Fig 1P). This suggested that Mbl
140 is not involved in the splicing fidelity of *Dscam2.10* but rather in the selective mutual
141 exclusion of its two isoforms. To assess whether the ratios of the two isoforms were
142 changing in the *mbl* hypomorphic mutants, we cut the exon 10 RT-PCR products with
143 the *ClaI* restriction enzyme that only recognizes exon 10A. Densitometric analysis
144 then allowed us to semi-quantitatively compare the relative levels of both isoforms.
145 There was ~25% increase in the level of exon 10A inclusion in $mbl^{e127}/mbl^{MI00976}$
146 animals compared to controls (Fig 1P). Similarly, qRT-PCR of the $mbl^{e127}/mbl^{MI00976}$
147 animals showed a ~1.25 fold and ~0.78 fold change in exon 10A and 10B inclusion
148 respectively, when compared to controls. Both results are consistent with the de-
149 repression we observed in our 10A reporter lines. To determine whether Mbl was
150 specifically regulating *Dscam2* exon 10 mutually exclusive splicing, we assessed

151 other *Dscam2* alternative splicing events. These included an alternative 5' splice site
152 selection of *Dscam2* exon 19 and the alternative last exon (ALE) selection of exon 20
153 (Fig S2A). The expression of these different isoforms was unchanged in *mbl*
154 hypomorphic mutants (Fig S2B). Together, our results indicate that Mbl is an
155 essential splicing factor that specifically represses *Dscam2.10A*.
156
157 **Mbl is necessary for the selection of *Dscam2* exon 10B**
158 Since *Dscam2* exon 10 isoforms are mutually exclusively spliced, we predicted that
159 selection of exon 10A would lead to the loss of exon 10B selection. To test this, we
160 conducted mosaic analysis with a repressible cell marker (MARCM) (Lee and Luo,
161 1999) to analyse *Dscam2.10B* expression in *mbl* mutant clones. In late third instar
162 brains, clones homozygous (GFP-positive) for mbl^{e127} and mbl^{e27} exhibited a dramatic
163 reduction in *Dscam2.10B>tdTom* expression in R cell axons projecting to the lamina
164 plexus compared to controls (Fig 2B, C, E). The absence of *Dscam2.10B>tdTom* in
165 *mbl* mutant clones was more striking during pupal stages (Fig 2D), suggesting that
166 perdurance of Mbl could explain the residual signal observed in third instar animals.
167 These results reveal that *mbl* is cell-autonomously required for the selection of the
168 *Dscam2.10B*.
169
170 ***mbl* expression is cell-type-specific and correlates with *Dscam2.10B* selection**
171 Previous studies have reported that *mbl* is expressed in third instar eye-discs and
172 muscles (Artero et al., 1998; Brouwer et al., 1997). Since *mbl* LOF results in both the
173 selection of *Dscam2.10A* and the loss of *Dscam2.10B*, we predicted that *mbl*
174 expression would correlate with the presence of isoform B. To test this, we
175 characterized several *mbl* reporters (Fig S3A). We analyzed three enhancer trap

176 strains (transcriptional reporters) inserted near the beginning of the *mbl* gene
177 (*mbl*^{k01212}*-LacZ*, *mbl*^{NP1161}*-Gal4* and *mbl*^{NP0420}*-Gal4*), as well as a splicing trap line
178 generated by the Trojan-mediated conversion of a *mbl* MiMIC (Minos Mediated
179 Integration Cassette) insertion (Fig S2A, *mbl*^{MiMIC00139}*-Gal4;* (Diao et al., 2015). The
180 splicing trap reporter consists of a splice acceptor site and an in-frame *T2A-Gal4*
181 sequence inserted in an intron between two coding exons. This *Gal4* cassette gets
182 incorporated into *mbl* mRNA during splicing and therefore Gal4 is only present when
183 *mbl* is translated. Consistent with previous studies, and its role in repressing the
184 production of *Dscam2.10A*, all four *mbl* reporters were expressed in the third instar
185 photoreceptors (Fig 3A, S3A-S3D). We next did a more extensive characterization of
186 *mbl* expression by driving nuclear localized GFP (*GFP.nls*) with one transcriptional
187 (*mbl*^{NP0420}*-Gal4)* and one translational (*mbl*^{MiMIC00139}*-Gal4)* reporter. In the brain, we
188 found that *mbl* was expressed predominantly in postmitotic neurons with some
189 expression detected in glial cells (Fig SEC-S3H and S3J-S3M). Interestingly, we
190 detected the translational but not the transcriptional reporter in third instar muscles
191 (Fig S3I and S3N). The absence of expression is likely due to the insertion of the *P-*
192 element into a neural-specific enhancer, as previously described (Bargiela et al.,
193 2014). To assess the expression of *mbl* in the five lamina neurons L1- L5, all of which
194 express *Dscam2* (Lah et al., 2014; Tadros et al., 2016), we implemented an
195 intersectional strategy using a *UAS>stop>epitope* reporter (Nern et al., 2015) that is
196 dependent on both *FLP* and *Gal4*. The *FLP* source (*Dac-FLP*) was expressed in
197 lamina neurons and able to remove the transcriptional stop motif in the reporter
198 transgene. The overlap between *mbl-Gal4* and *Dac-FLP* allowed us to visualize *mbl*
199 expression in lamina neurons at single-cell resolution (Fig 3B). As a proof of
200 principle, we first did an intersectional analysis with a pan-neuronal reporter, *elav-*

201 *Gal4* (Fig 3C$_1$). We detected many clones encompassing various neuronal-cell-types
202 including the axons of L1-L5 and R7-R8 (Fig 3C-3D). This confirmed that all lamina
203 neurons could be detected using this strategy. Using *mbl-Gal4* reporters we found
204 that L1, R7 and R8, which expresses *Dscam2.10B*, were the primary neurons labelled.
205 A few L4 cells were also detected, which is consistent with this neuron expressing
206 *Dscam2.10B* early in development and *Dscam2.10A* at later stages (Tadros et al.,
207 2016). To confirm this finding, we dissected the expression of *mbl* in lamina neurons
208 during development. Using the same intersectional strategy, we detected a high
209 number of L4 clones at 48hr apf (30%, n=10). This was followed by a decline at 60hr
210 apf (26.7%, n = 30) and 72hr apf (11.8%, n = 85) reaching the lowest at eclosion (Fig
211 S4A and S4B;1.7%, n=242). Thus, *mbl* expression in L4 neurons mirrors the
212 expression of *Dscam2.10B*. Consistent with this, L2, L3 and L5, were all detected
213 using the intersectional strategy with *Dscam2.10A-Gal4* but were not labelled using
214 *mbl-Gal4* (Fig 3E). The expression of *mbl* is further strengthened by an independent
215 RNA-seq study of isolated lamina neurons during development, where *mbl* is detected
216 at high levels in L1, R7 and R8 neurons (~5-100 fold more than L2-L5)(Tan et al.,
217 2015). Together, these results show *mbl* expression correlates with the cell-type-
218 specific alternative splicing of *Dscam2.10B*. Importantly, this suggests that simply the
219 presence or absence of *mbl* can determine the selection of the *Dscam2.10* isoform in a
220 cell.
221
222 **Ectopic expression of multiple *mbl* isoforms is sufficient to promote the selection**
223 **of *Dscam2* exon 10B**
224 Since cells that select *Dscam2.10B* express *mbl* and cells that select *Dscam2.10A* lack
225 *mbl*, we wondered whether it was sufficient to promote exon 10B selection in

226 *Dscam2.10A*-positive cells. To test this, we ectopically expressed *mbl* with a
227 ubiquitous driver (*Act5c-Gal4*) and monitored isoform B expression using
228 *Dscam2.10B>tdTom*. We focussed on the mushroom body (MB), as this tissue
229 expresses isoform A specifically in α'β' neurons at 24hr apf where *mbl* is not
230 detected (Fig 3G-3H, 4A-4C). Consistent with our prediction, ectopic expression of
231 *mbl* using an enhancer trap containing a *UAS* insertion at the 5' end of the gene
232 (*Act5c>mbl*$^{B2\text{-}E1}$), switched on *Dscam2.10B* in α'β' MB neurons, where it is normally
233 absent (Fig 4D). Driving *mbl* with a MB-specific *Gal4* (*OK107*) gave similar results
234 (Fig 4E). Although our two *Gal4* drivers expressed *mbl* in all MB neurons,
235 *Dscam2.10B* was only observed in α'β' neurons, demonstrating that transcription of
236 *Dscam2* is a pre-requisite for this splicing modulation. Previous studies have
237 suggested that the *mbl* gene is capable of generating different isoforms with unique
238 functions depending on their subcellular localization (Vicente et al., 2007). This also
239 includes the production of a highly abundant circular RNA that can sequester the Mbl
240 protein (Ashwal-Fluss et al., 2014; Houseley et al., 2006). To assess whether *Dscam2*
241 exon 10B selection is dependent on a specific alternative variant of Mbl, we
242 overexpressed the cDNAs of fly *mbl* isoforms (*mblA*, *mblB* and *mblC*; (Begemann et
243 al., 1997; Juni and Yamamoto, 2009) as well as an isoform of the human *MBNL1* that
244 lacks the linker region optimal for CUG repeat binding (*MBNL1*$_{35}$; (Kino et al., 2004;
245 Li et al., 2008) with either *Act5c-Gal4* or *OK107-Gal4*. These constructs all possess
246 the tandem N-terminal CCCH motif that binds to YCGY sequences and lack the
247 ability to produce *mbl* circRNA. In all cases, overexpression resulted in the
248 misexpression of *Dscam2.10B* in α'β' MBs (with the exception *Act5C>mblC*, which
249 resulted in lethality; Fig 4D-4E). Using semi-quantitative RT-PCR from the
250 *Act5C>mbl* flies, we demonstrated that overexpression of *mbl* did not lead to exon 10

251 skipping and that it increased exon 10B selection by 8-24% (Fig 4F), depending on
252 the *mbl* isoform used. The inability of Mbl to completely inhibit exon 10A selection
253 suggests that other factors or mechanisms may also contribute to cell-specific *Dscam2*
254 isoform expression (see Discussion). These results suggest that Mbl protein isoforms
255 are all capable of *Dscam2.10B* selection and independent of *mbl* circRNA. The ability
256 of human MBNL1 to promote the selection of exon 10B suggests that the regulatory
257 logic for *Dscam2* splicing is likely conserved in other mutually-exclusive cassettes in
258 higher organisms. Together, our results show that all *mbl* isoforms are sufficient to
259 promote *Dscam2.10B* selection.
260

261 **Mbl regulates cell-type-specific *Dscam2* alternative splicing in lamina neurons**

262 To determine whether the regulatory logic of *Dscam2* alternative splicing is consistent
263 in other cell types, we manipulated *mbl* expression in lamina neurons (L1-L5). We
264 first asked whether *mbl* LOF resulted in the de-repression of *Dscam2.10A* in L1
265 neurons. To do this, we visualized *Dscam2* isoform expression in L1-L5 using an
266 intersectional strategy similar to Figure 3 but with a different *FLP* source (*27G05-*
267 *FLP*). We detected L1 and L4 neurons when using the *Dscam2.10B-Gal4* reporter in a
268 wild-type background, but not L2, L3 or L5. L1 was also not detected when using the
269 *Dscam2.10A-Gal4* reporter, where L2-L5 cells were the primary neurons labelled (Fig
270 5A). Consistent with our R cell results, de-repression of *Dscam2.10A* was observed in
271 L1 neurons in *mbl* transheterozygous animals ($mbl^{e127}/mbl^{MI00976}$) when compared to
272 the corresponding heterozygous controls (mbl^{e127}/+ and $mbl^{MI00976}$/+, Fig 5A-5B). We
273 next asked whether ectopic overexpression of *mbl* would result in aberrant
274 *Dscam.10B* selection in L2, L3 and L5 neurons where it is usually repressed. For this
275 experiment, the *Gal4/UAS* system was used to overexpress *mbl* and the *LexA/LexAop*

276 system was used to visualize *Dscam2* isoform expression. Using the same
277 intersectional strategy, we found that *Dscam2-LexA* reporters showed similar patterns
278 to the *Dscam2-Gal4* reporters (Fig 5C). Pan-neuronal overexpression (*elav-Gal4*) of
279 *mbl* caused the aberrant detection of *Dscam2.10B* in L2, L3 and L5 cells that
280 normally select *Dscam2.10A* (Fig 5C-5D). Together, our results show that Mbl
281 regulates *Dscam2* cell-type-specific alternative splicing. Importantly, the simple
282 presence or absence of *mbl* is sufficient to determine whether a cell expresses
283 *Dscam2.10A* or *Dscam2.10B*.
284
285 **Manipulation of *mbl* expression generates phenotypes observed in *Dscam2* single**
286 **isoform mutants**
287 If Mbl regulates *Dscam2* alternative splicing, *mbl* LOF and OE animals should exhibit
288 similar phenotypes to *Dscam2* isoform misexpression. Previously, we showed that
289 flies expressing a single isoform of *Dscam2* exhibit a reduction in L1 axon arbour size
290 and well as reduced dendritic width (Kerwin et al., 2018; Lah et al., 2014). These flies
291 were generated using recombinase-mediated cassette exchange and express a single
292 isoform in all *Dscam2*-positive cells (Lah et al., 2014). The reduction in axonal arbors
293 and dendritic widths were proposed to be due to inappropriate interactions between
294 cells that normally express different isoforms. Consistent with these previous studies,
295 we observed a reduction in the area of L1 axon arbors (more prominent in m1 than in
296 m5, Fig 5E-5F and 5I-5J) and the width of dendritic arrays (Fig 5G-5H and 5G) in
297 *mbl* transheterozygous animals ($mbl^{e127}/mbl^{MI00976}$) when compared to controls. Finally,
298 we observed a phenotype in MB neurons overexpressing *mbl* where the β lobe
299 neurons inappropriately crossed the midline (Fig S5A-S5C). Interestingly, a similar
300 phenotype was observed in *Dscam2A* single isoform mutants. These data demonstrate

301 that MB phenotypes generated in animals overexpressing *mbl*, phenocopy *Dscam2*
302 single isoform mutants. While the origin of this non-autonomous phenotype is not
303 known, it correlates with the misregulation of *Dscam2* alternative isoform expression.
304

305 **Discussion**

306 In this study, we identify Mbl as a regulator of *Dscam2* alternative splicing. We
307 demonstrate that removing *mbl* in a *mbl*-positive cell-type results in a switch from
308 *Dscam2.10B* to *Dscam2.10A* selection. Ectopic expression of a variety of Mbl protein
309 isoforms in a normally *mbl*-negative neuronal cell-type is sufficient to trigger the
310 selection of *Dscam2.10B*. Consistent with this, transcriptional reporters demonstrate
311 that *mbl* is expressed in a cell-type-specific manner in multiple cell-types, which
312 tightly correlates with *Dscam2.10B*. Lastly, both *mbl* LOF and misexpression lead to
313 phenotypes that are observed in flies that express a single *Dscam2* isoform.
314

315 Our data demonstrate that *mbl* is expressed in a cell-specific fashion. In the lamina of
316 the fly visual system, L1 and L2 neurons are developmentally very similar in terms of
317 both morphology and gene expression (Bausenwein et al., 1992; Fischbach and
318 Dittrich, 1989; Tan et al., 2015). The difference in *mbl* expression between these two
319 cells is critical for their development as when expression of this splicing factor is
320 perturbed, both cells express the same isoforms and inappropriate Dscam2
321 interactions lead to phenotypes in their axons and dendrites. Although, cell-specific
322 *mbl* expression has been alluded to previously (Huang et al., 2008; Machuca-Tzili et
323 al., 2011; Norris et al., 2017), our study demonstrates that *mbl* regulation of *Dscam2*
324 alternative splicing has functional consequences. Mbl appears to be regulated at the
325 transcriptional level since the enhancer-trap as well as splicing-trap reporters lack the

326 components crucial for post-transcriptional regulation yet still exhibit cell-type-
327 specific expression (Fig 3). This was unexpected as a recent study showed that *mbl*
328 encodes numerous alternative isoforms that could be individually post-
329 transcriptionally repressed by different microRNAs, thus bypassing the need for
330 transcriptional control of the gene. It will be interesting to explore the *in vivo*
331 expression patterns of other splicing factors in *Drosophila* to determine whether cell-
332 specific expression of a subset of splicing factors is a common mechanism for
333 regulating alternative splicing in the brain.
334
335 The expression pattern of *mbl* and its ability to simultaneously repress exon 10A and
336 select exon 10B suggest that this RNA binding protein and its associated co-factors
337 are sufficient to regulate cell-type-specific splicing of *Dscam2*. *Dscam2.10A* could be
338 the default exon selected when the Mbl complex is absent. In this way, cells that
339 express *mbl* select *Dscam2.10B*. Consistent with this, ectopic expression of *mbl* in
340 *mbl*-negative cells (L2, L3, L5 & α'β' neurons) results in the aberrant selection of
341 exon 10B. Our RT-PCR data, however, argue that *Dscam2* mutually exclusive
342 alternative splicing may be more complicated than this model. Ubiquitous expression
343 of *mbl* increased exon B inclusion modestly (up to 24%) as measured by RT-PCR
344 (see Fig 4F). One might expect a more pronounced shift to isoform B if Mbl were the
345 only regulator/mechanism involved. Further studies, including screens for repressors
346 of exon 10B, will be required to resolve this issue.
347
348 The L1 axon and dendrite phenotypes generated through the LOF and ectopic
349 expression of *mbl*, respectively, demonstrate that this splicing factor regulates aspects
350 of neurodevelopment through cell-specific expression of *Dscam2* isoforms. In the

351 lamina, *mbl* expression in L1, and its absence in L2, permits these neurons to express
352 distinct Dscam2 proteins that cannot recognise each other. Phenotypes arise in these
353 neurons both when they are engineered to express the same isoform (Kerwin et al.,
354 2018; Lah et al., 2014) and when mbl is misregulated (Fig 5). These data strongly link
355 the regulation of cell-specific *Dscam2* splicing with normal neuron development.
356 *Mbl* overexpression also generates a midline crossing phenotype in MB neurons that
357 is similar to that observed in animals expressing a single isoform. This phenotype is
358 complicated, however, by the observation that *Dscam2.10A*, but not *Dscam2.10B*,
359 animals show a statistically significant increase in midline crossing compared to
360 controls (Fig S4). This issue may have to do with innate differences between isoform
361 A and isoform B that are not completely understood. It is possible that isoform A and
362 B are not identical in terms of signalling due to either differences in homophilic
363 binding or differences in co-factors associated with specific isoforms. Consistent with
364 this notion, we previously reported that *Dscam2.10A* single isoform lines produce
365 stronger phenotypes at photoreceptor synapses compared to *Dscam2.10B* (Kerwin et
366 al., 2018).
367
368 Together, our results demonstrate that the simple presence or absence of a splicing
369 factor can affect neurodevelopment through the cell-specific selection of distinct
370 isoforms of a cell surface protein. Although we provide compelling genetic evidence
371 of how Mbl regulates the alternative splicing of *Dscam2*, the regulatory logic we
372 discovered for *Dscam2* is likely to extend to cover the splicing events of many other
373 genes crucial for neurodevelopment. Developmental analysis of *mbl* expression in the
374 cells studied here suggests that it turns on after neurons have obtained their identity
375 (similar to *Dscam2*) and is therefore well suited for regulating processes such as axon

376 guidance and synapse specification. Identifying these splicing events may provide
377 clues into how the brain can diversify and regulate its repertoire of proteins to
378 promote neural connectivity.
379

380 **Experimental procedures**

381 **Fly strains**

382 *Dscam2.10A-LexA* and *Dscam2.10B-LexA* (Tadros et al., 2016), *UAS-Dcr2* and *UAS-*
383 *mbl-RNAi*^{VDRC28732} (Dietzl et al., 2007), *LexAop-myr-tdTomato* (attP2, (Chen et al.,
384 2014), *UAS-Srp54-RNAi*$^{TRiP.HMS03941}$, *CadN-RNAi*$^{TRiP.HMS02380}$ and *UAS-mbl-*
385 *RNAi*$^{TRiP.JF03264}$(Ni et al., 2008), *UAS-mCD8-GFP* (Lee and Luo, 1999), *FRT42D* (Xu
386 and Rubin, 1993), *mbl*^{e127} and *mbl*^{e27}(Begemann et al., 1997), *mbl*^{MI00976} and *mbl*^{MI04093}
387 (Venken et al., 2011), *Df(2R)BSC154* (Cook et al., 2012), *Df(2R)Exel6066* (Parks et
388 al., 2004), *ey-FLP* (Chr.1, (Newsome et al., 2000), *GMR-myr-GFP*, *mbl*^{NP0420}*-Gal4*
389 and *mbl*^{NP1161}*-Gal4* (Hayashi et al., 2002), *mbl*^{k01212}*-LacZ* (Spradling et al., 1999),
390 *mbl*^{MiMIC00139}*-Gal4* (H. Bellen Lab), *Dac-FLP* (Chr.3, (Millard et al., 2007),
391 *UAS>stop>myr::smGdP-V5-THS-UAS>stop>myr::smGdP-cMyc* (attP5, (Nern et al.,
392 2015), *Dscam2.10A-Gal4* and *Dscam2.10B-Gal4* (Lah et al., 2014) *Act5C-Gal4*
393 (Chr.3, from Yash Hiromi), *OK107-Gal4* (Connolly et al., 1996), *UAS-mblA*, *UAS-*
394 *mblB* and *UAS-mblC* (D. Yamamoto Lab), *P{EP}mbl*$^{B2-E1}$, *UAS-mblA-FLAG* and
395 *UAS-MBNL1*$_{35}$ (Li et al., 2008).
396

397 **RNAi screening**

398 The RNAi screen line was generated as follows: *GMR-Gal4* was recombined with
399 *GMR-GFP* on the second chromosome. *Dscam2.10A-LexA* (Tadros et al. 2016) was
400 recombined with *LexAop-myr-tdTomato* on the third chromosome. These flies were

401 crossed together with *UAS-Dcr-2* (X) to make a stable RNAi screen stock. UAS-
402 RNAi lines were obtained from Bloomington and VDRC. Lethal UAS-RNAi stocks
403 were placed over balancers with developmentally selectable markers. Virgin females
404 were collected from the RNAi screen stock, crossed to UAS-RNAi males and reared
405 at 25°C. Wandering third instar larvae were dissected and fixed. We tested between
406 one to three independent RNAi lines per gene. In total, we imaged ~2300 third instar
407 optic lobes without antibodies using confocal microscopy at 63X. RNAi lines tested
408 are listed in Table S1.
409
410 **Semiquantitative and quantitative RT-PCR**
411 Total RNA was isolated using TRIzol (Ambion) following the manufacturer's
412 protocol. Reverse transcription was performed on each RNA sample with random
413 primer mix (semiquantitative, NEB) or Oligo-dT (qRT-PCR, NEB) using 200 units of
414 M-MULV (NEB) and 1 μg of RNA in a 20 μL reaction, at 42°C for 1 hr. PCR
415 reactions were set up with specific primers to analyse alternative splicing of various
416 regions of *Dscam2*. Where possible, semi-quantitative PCR was performed to
417 generate multiple isoforms in a single reaction and relative levels were compared by
418 electrophoresis followed by densitometry. For qRT-PCR, 1μL of CDNA were added
419 to a Luna Universal SYBR-Green qPCR Master Mix kit (NEB). Samples were added
420 into a 200μL 96-well plate and read on the QuantStudio TM 6 Flex Real-Time PCR
421 machine. Rq values were calculated in Excel (Microsoft).
422
423 **Immunohistochemistry**
424 Immunostaining were conducted as previously described (Lah et al. 2014). Antibody
425 dilutions used were as follows: mouse mAb24B10 (1:20; DSHB), mouse anti-Repo

426 (1:20; DSHB), mouse anti-DAC (1:20; DSHB), mouse anti-Fas2 (1:20; DSHB) rat
427 anti-ELAV (1:200), V5-tag:DyLight anti-mouse 550 (1:500; AbD Serotec), V5-
428 tag:DyLight anti-mouse 405 (1:200; AbD Serotec), myc-tag;DyLight anti-mouse 549
429 (1:200; AbD Serotec), Phalloidin:Alexa Fluor 568 (1:200; Molecular Probes),
430 DyLight anti-mouse 647 (1:2000; Jackson Laboratory), DyLight Cy3 anti-rat (1:2000;
431 Jackson Laboratory).
432
433 **Image acquisition**
434 Imaging was performed at the School of Biomedical Sciences Imaging Facility.
435 Images were taken on a Leica SP8 laser scanning confocal system with a 63X
436 Glycerol NA 1.3.
437
438 **Fly genotypes**
439 Specific genotypes can be found in the supplemental text.
440
441 **Author contribution**
442 J.S.S.L designed and performed all experiments. S.S.M supervised the project. J.S.S.L
443 and S.S.M wrote the manuscript.
444
445 **Acknowledgements**
446 We thank Wael Tadros, Yi Chen, Larry Zipursky, Greg Neely, Louis O'Keefe, Nancy
447 Bonini, Aljoscha Nern and Bloomington Stock Center for sharing fly stocks. We
448 thank the Daisuke Yamamoto Lab for constructing the *UAS-mbl* lines deposited and
449 maintained at the Kyoto Stock Center. We thank Shaun Walters for technical
450 assistance on the Leica confocal microscopy. We note that Grace Shin initially

observed *Dscam2* isoform expression in the adult mushroom bodies. We thank Kevin Mutemi for his thorough characterization of *Dscam2* isoform expression in mushroom bodies during development and all midline crossing defects in *Dscam2* single isoform mutant animals. We thank Wei Jun Tan for the heroic feat of triple balancing *OK107-Gal4*. We also thank members of the Millard, Pecot, Hilliard and van Swinderen lab for their feedback. The RNAi screen was inspired by the works of Hidehito Kuroyanagi. This work was supported by the National Health and Medical Research Council of Australia (NHMRC grant APP1021006). J.S.S.L was supported by the Australia Postgraduate Award (Research Training Scheme) from the Australian Federal Government and the Lavidis grant in aid.

463 **Figure legends**

464 **Figure 1.** *Drosophila mbl* is required for the repression of *Dscam2* exon 10A in R
465 cells. (A) Schematic showing the region of *Dscam2* exon 10 that undergoes mutually
466 exclusive alternative splicing and the LexA isoform-specific reporter lines. Frame-
467 shift mutations in the exon not reported are shown. (B) Schematic RNAi screen
468 design for identifying repressors of *Dscam2* exon 10A selection. R cells normally
469 select exon 10B and repress exon 10A. We knocked-down RNA binding proteins in R
470 cells while monitoring 10A expression.

471 (C-E) *Dscam2* exon 10A is derepressed in R cells when *mbl* is knocked-down. (C_1-C_3)
472 *Dscam2.10B* control. R cells (green) normally select exon 10B (red). R cell terminals
473 can be observed in the lamina plexus (angle brackets). *Dscam2.10B* is also expressed
474 in the developing optic lobe (arrowhead). (D_1-D_3) *Dscam2.10A* is not expressed in R
475 cells (green) but is expressed in the developing optic lobe (arrowhead). (E_1-E_3) RNAi
476 lines targeting *mbl* in R cells results in the aberrant expression of *Dscam2.10A* in R
477 cells.

478 (F) Schematic of the *mbl* gene showing the location of two small deletions (*E27* and
479 *E127*), two MiMIC insertions (*MI04093* and *MI00976*) and two deficiencies
480 (*Df(2R)Exel6066 and Df(2R)BSC154*) used in this study. Non-coding exons are in
481 gray, coding exons are black.

482 (G) Complementation test of *mbl* loss-of-function (LOF) alleles. Numbers in the table
483 represent the number of non-*CyO* offspring over the total. Most transheterygote
484 combinations were lethal with the exception of $mbl^{MI00976}/mbl^{e27}$ and
485 $mbl^{MI00976}/mbl^{MI04093}$ (green).

486 (H-N) *Mbl* transheterozygotes express *Dscam2.10A* in R cells. (H) *Dscam2.10B*
487 control showing expression in the lamina plexus (angle brackets). (I) *Dscam2.10A*

488 control showing no expression of this isoform in R cells. (J-L) Heterozygous animals
489 for *mbl* LOF alleles are comparable to control. (M-N) Two different *mbl*
490 transheterozygote combinations exhibit de-repression of *Dscam2.10A* in R cells.
491 (O) Quantification of *Dscam2.10>tdTom* expression in third instar R cells with
492 various *mbl* manipulations; including RNAi knockdown (black bars) and whole
493 animal transheterozygotes (white). Y-axis represents the number of optic lobes with R
494 cells positive for tdTom over total quantified as a percentage. On the x-axis, the
495 presence of a transgene is indicated with a grey box and the temperature at which the
496 crosses were reared (25°C or 29°C) is indicated on the top.
497 (P) *Dscam2* exon 10A inclusion is increased in *mbl* transheterozygotes. (Top)
498 Semiquantitative RT-PCR from different genotypes indicated. Primers amplified the
499 variable region that includes exon 10. A smaller product that would result from exon
500 10 skipping is not observed. (Bottom) Exon 10A-specific cleavage with restriction
501 enzyme ClaI shows an increase in exon 10A inclusion in *mbl* transheterozygotes.
502 Percentage of exon 10A inclusion was calculated by dividing 10A by 10A+10B bands
503 following restriction digest. The mean of exon 10A inclusion is shown at the bottom
504 of each lane. ANOVA test with Tukey's multiple comparison test was used to
505 compare the exon 10A inclusion. ns $P > 0.05$, ** $P < 0.01$. See also Figures S1 and
506 S2.
507
508 **Figure 2.** *Drosophila mbl* is necessary for the selection of *Dscam2* exon 10B in R
509 cells.
510 (A) Schematic of our predicted *mbl* MARCM results using *ey-FLP*. WT R cell clones
511 will be GFP(+) and *Dscam2.10B>tdTom*(+) (yellow), whereas *mbl* mutant clones will
512 be *Dscam2.10B>tdTom*(-) (green). (B_1-B_3) Control MARCM clones (green) in 3rd

513 instar R cells (angle brackets) are positive for *Dscam2.10B>tdTom* (arrowhead). (C_1-
514 C_3) In *mbl*^{e27} clones, *Dscam2.10B* labelling in the lamina plexus is discontinuous and
515 its absence correlates with the loss of Mbl (arrowhead). (D_1-D_2) *Mbl* MARCM clones
516 from midpupal optic lobes lack *Dscam2.10B*>tdTom. (E_1-E_3) A different allele
517 (*mbl*^{e127}) exhibits a similar phenotype in third instar brains.
518
519 **Figure 3**. *mbl* is expressed in a cell-specific manner that correlates with *Dscam2.10B*
520 (A) A *mbl-Gal4* reporter (green) is expressed in third instar R cells but not in lamina
521 neuron precursor cells labelled with an antibody against Dacshund (DAC, red).
522 (B) Schematic of MultiColor FlpOut (MCFO) approach to characterize *mbl* reporter
523 expression in lamina neurons at adult stages. The UAS FlpOut construct produces an
524 epitope-tagged version of a non-fluorescent GFP (smGFP,(Nern et al., 2015))
525 (C_1-C_4) All lamina neurons can be detected using a MCFO strategy with a pan-
526 neuronal reporter (*elav-Gal4*). Lamina neurons were identified based on their unique
527 axon morphologies. (D_1-D_4) An intersectional strategy using *mbl-Gal4* labels
528 primarily L1 lamina neurons. (E) Quantification of lamina neurons and R7-R8
529 neurons observed using the intersectional strategy. Dark green and light green boxes
530 represent high and low numbers of labelled neurons, respectively. (F-H) *Mbl* is not
531 expressed in mushroom body (MB) neurons that express *Dscam2.10A* at 24hr apf.
532 (F_1-F_2) *Dscam2.10A* is expressed in α'β' MB neurons that are not labelled by Fas2.
533 Fas2 labels the αβ and γ subsets of MB neurons. (G-H) Neither *Dscam2.10B* (G_1-G_2)
534 nor *mbl* (H_1-H_2) are detected in MB neurons. See also Figures S3 and S4.
535
536 **Figure 4.** Multiple *mbl* isoforms promte selection of *Dscam2* exon 10B

537 (A) Schematic showing that *mbl* is sufficient to drive *Dscam2.10B* selection in
538 α'β'neurons.
539 (B) Control showing that *Dscam2.10A* (red) is expressed in α'β' neurons at 24hr apf.
540 (C) Control showing that *Dscam2.10B* is normally repressed in α'β' neurons. (D)
541 Overexpression of *mbl* activates *Dscam2.10B* selection (red) in α'β' neurons. (E)
542 Quantification of *Dscam2.10* expression in α'β' neurons at 24-36hr apf with and
543 without *mbl* OE. Control (No Gal4, grey bar), ubiquitous driver (*Act5c-Gal4*, black
544 bars) and pan-mushroom body neuron driver (*OK107-Gal4*, white bars). Y-axis
545 represents the number of tdTom positive (+) α'β' over the total, expressed as a
546 percentage. Ratio of tdTom(+)/total is shown in each bar. (F) *Mbl* OE increases
547 *Dscam2* exon 10B inclusion. Semiquantitative RT-PCR as in Figure 1. Exon 10A-
548 specific cleavage with restriction enzyme ClaI shows an increase in exon 10B
549 inclusion in *mbl* OE animals, without exon 10 skipping. Percentage of exon 10B
550 inclusion was calculated by dividing 10B by 10A+10B bands following
551 electrophoresis and densitometry. The mean of exon 10B inclusion is shown at the
552 bottom of each lane. ANOVA test with Tukey's multiple comparison test was used to
553 compare the exon 10B inclusion. ns $P > 0.05$, ** $P < 0.01$, *** $P < 0.001$.
554
555 **Figure 5.** Mbl regulates *Dscam2* cell-type-specific alternative splicing in lamina
556 neurons.
557 (A) Quantification of lamina neurons L1-L5 observed using the *Dscam2.10B-Gal4*
558 (magenta) or *Dscam2.10A-Gal4* (blue) reporters with the intersectional strategy in
559 *mbl* LOF animals. Green boxes represent high number of labelled neurons.
560 *Dscam2.10A* is de-repressed in L1 neurons in a *mbl* LOF background
561 ($mbl^{MI00976}/mbl^{e27}$, hash tag).

562 (B) Schematic of *Dscam2.10A* de-repression in *mbl* LOF L1 neurons.

563 (C) Quantification of lamina neurons L1-L5 observed using the *Dscam2.10A-LexA*

564 (blue) or *Dscam2.10B-LexA* (magenta) reporters with the intersectional strategy in

565 animals with pan-neuronal (*elav-Gal4*) expression of *mbl*. Green boxes represent high

566 numbers of labelled neurons. *Dscam2.10B-LexA* was aberrantly detected in L2, L3

567 and L5 neurons overexpressing *mblB* (hash tag).

568 (D) Schematic of aberrant *Dscam2.10B* selection in L2, L3 and L5 neurons

569 overexpressing *mbl*.

570 (E-K) L1 neurons in *mbl* LOF animals have reduced axon arbor area and dendritic

571 array width when compared to controls. (E) A representative confocal image of a

572 control L1 axon (green) with arbors at m1 and m5 layers. (F) A representative

573 confocal image of an L1 axon from *mbl* LOF animals ($mbl^{MI00976}/mbl^{e27}$). (G) A

574 representative confocal image of a control L1 dendritic array (grey). (H) A

575 representative confocal image of a L1 dendritic array from *mbl* LOF animals

576 ($mbl^{MI00976}/mbl^{e27}$). (I) Quantification of L1 axon m1 arbor area (mm^2). (J)

577 Quantification of L1 axon m5 arbor area (mm^2). (K) Quantification of L1 dendritic

578 width (mm). Tukey boxplot format: middle line = median, range bars = min and max,

579 box = 25–75% quartiles, and each data point = single cartridge. Numbers in

580 parentheses represent total number of L1 neurons quantified. Parametric t-test was

581 used to compare *mbl* LOF L1 axon arbour area with controls. Non-parametric t-test

582 was used to compare *mbl* LOF L1 dendritic width with controls. **** $P<0.0001$.

583 Bars, 5mm (E-H).

584

585

586

587 **References**

588 Artero, R., Prokop, A., Paricio, N., Begemann, G., Pueyo, I., Mlodzik, M., Perez-
589 Alonso, M., and Baylies, M.K. (1998). The muscleblind gene participates in the
590 organization of Z-bands and epidermal attachments of Drosophila muscles and is
591 regulated by Dmef2. Developmental biology 195, 131-143.

592 Ashwal-Fluss, R., Meyer, M., Pamudurti, N.R., Ivanov, A., Bartok, O., Hanan, M.,
593 Evantal, N., Memczak, S., Rajewsky, N., and Kadener, S. (2014). circRNA
594 biogenesis competes with pre-mRNA splicing. Molecular cell 56, 55-66.

595 Bargiela, A., Llamusi, B., Cerro-Herreros, E., and Artero, R. (2014). Two enhancers
596 control transcription of Drosophila muscleblind in the embryonic somatic
597 musculature and in the central nervous system. PloS one 9, e93125.

598 Bausenwein, B., Dittrich, A.P., and Fischbach, K.F. (1992). The optic lobe of
599 Drosophila melanogaster. II. Sorting of retinotopic pathways in the medulla. Cell
600 and tissue research 267, 17-28.

601 Begemann, G., Paricio, N., Artero, R., Kiss, I., Perez-Alonso, M., and Mlodzik, M.
602 (1997). muscleblind, a gene required for photoreceptor differentiation in
603 Drosophila, encodes novel nuclear Cys3His-type zinc-finger-containing proteins.
604 Development 124, 4321-4331.

605 Bell, T.J., Thaler, C., Castiglioni, A.J., Helton, T.D., and Lipscombe, D. (2004). Cell-
606 specific alternative splicing increases calcium channel current density in the pain
607 pathway. Neuron 41, 127-138.

608 Blanchette, M., Green, R.E., MacArthur, S., Brooks, A.N., Brenner, S.E., Eisen, M.B.,
609 and Rio, D.C. (2009). Genome-wide analysis of alternative pre-mRNA splicing and
610 RNA-binding specificities of the Drosophila hnRNP A/B family members.
611 Molecular cell 33, 438-449.

612 Brand, A.H., and Perrimon, N. (1993). Targeted gene expression as a means of
613 altering cell fates and generating dominant phenotypes. Development 118, 401-
614 415.

615 Brouwer, J., Nagelkerke, D., den Heijer, P., Ruiter, J.H., Mulder, H., Begemann, M.J.,
616 and Lie, K.I. (1997). Analysis of atrial sensed far-field ventricular signals: a
617 reassessment. Pacing and clinical electrophysiology : PACE 20, 916-922.

618 Calarco, J.A., Superina, S., O'Hanlon, D., Gabut, M., Raj, B., Pan, Q., Skalska, U.,
619 Clarke, L., Gelinas, D., van der Kooy, D., *et al.* (2009). Regulation of vertebrate
620 nervous system alternative splicing and development by an SR-related protein.
621 Cell 138, 898-910.

622 Chen, Y., Akin, O., Nern, A., Tsui, C.Y., Pecot, M.Y., and Zipursky, S.L. (2014). Cell-
623 type-specific labeling of synapses in vivo through synaptic tagging with
624 recombination. Neuron 81, 280-293.

625 Connolly, J.B., Roberts, I.J., Armstrong, J.D., Kaiser, K., Forte, M., Tully, T., and
626 O'Kane, C.J. (1996). Associative learning disrupted by impaired Gs signaling in
627 Drosophila mushroom bodies. Science 274, 2104-2107.

628 Cook, R.K., Christensen, S.J., Deal, J.A., Coburn, R.A., Deal, M.E., Gresens, J.M.,
629 Kaufman, T.C., and Cook, K.R. (2012). The generation of chromosomal deletions
630 to provide extensive coverage and subdivision of the Drosophila melanogaster
631 genome. Genome biology 13, R21.

632 Diao, F., Ironfield, H., Luan, H., Diao, F., Shropshire, W.C., Ewer, J., Marr, E., Potter,
633 C.J., Landgraf, M., and White, B.H. (2015). Plug-and-play genetic access to
634 drosophila cell types using exchangeable exon cassettes. Cell reports 10, 1410-
635 1421.

636 Dietzl, G., Chen, D., Schnorrer, F., Su, K.C., Barinova, Y., Fellner, M., Gasser, B.,
637 Kinsey, K., Oppel, S., Scheiblauer, S.*, et al.* (2007). A genome-wide transgenic
638 RNAi library for conditional gene inactivation in Drosophila. Nature 448, 151-
639 U151.

640 Fischbach, K.F., and Dittrich, A.P.M. (1989). The Optic Lobe of Drosophila-
641 Melanogaster .1. A Golgi Analysis of Wild-Type Structure. Cell and tissue research
642 258, 441-475.

643 Funada, M., Hara, H., Sasagawa, H., Kitagawa, Y., and Kadowaki, T. (2007). A
644 honey bee Dscam family member, AbsCAM, is a brain-specific cell adhesion
645 molecule with the neurite outgrowth activity which influences neuronal wiring
646 during development. The European journal of neuroscience 25, 168-180.

647 Hayashi, S., Ito, K., Sado, Y., Taniguchi, M., Akimoto, A., Takeuchi, H., Aigaki, T.,
648 Matsuzaki, F., Nakagoshi, H., Tanimura, T.*, et al.* (2002). GETDB, a database
649 compiling expression patterns and molecular locations of a collection of Gal4
650 enhancer traps. Genesis 34, 58-61.

651 Houseley, J.M., Garcia-Casado, Z., Pascual, M., Paricio, N., O'Dell, K.M., Monckton,
652 D.G., and Artero, R.D. (2006). Noncanonical RNAs from transcripts of the
653 Drosophila muscleblind gene. The Journal of heredity 97, 253-260.

654 Huang, H., Wahlin, K.J., McNally, M., Irving, N.D., and Adler, R. (2008).
655 Developmental regulation of muscleblind-like (MBNL) gene expression in the
656 chicken embryo retina. Developmental dynamics : an official publication of the
657 American Association of Anatomists 237, 286-296.

658 Iijima, T., Iijima, Y., Witte, H., and Scheiffele, P. (2014). Neuronal cell type-specific
659 alternative splicing is regulated by the KH domain protein SLM1. The Journal of
660 cell biology 204, 331-342.

661 Irion, U. (2012). Drosophila muscleblind codes for proteins with one and two
662 tandem zinc finger motifs. PloS one 7, e34248.

663 Juni, N., and Yamamoto, D. (2009). Genetic analysis of chaste, a new mutation of
664 Drosophila melanogaster characterized by extremely low female sexual
665 receptivity. Journal of neurogenetics 23, 329-340.

666 Kania, A., Salzberg, A., Bhat, M., D'Evelyn, D., He, Y., Kiss, I., and Bellen, H.J. (1995).
667 P-element mutations affecting embryonic peripheral nervous system
668 development in Drosophila melanogaster. Genetics 139, 1663-1678.

669 Kerwin, S.K., Li, J.S.S., Noakes, P.G., Shin, G.J., and Millard, S.S. (2018). Regulated
670 Alternative Splicing of Drosophila Dscam2 Is Necessary for Attaining the
671 Appropriate Number of Photoreceptor Synapses. Genetics 208, 717-728.

672 Kino, Y., Mori, D., Oma, Y., Takeshita, Y., Sasagawa, N., and Ishiura, S. (2004).
673 Muscleblind protein, MBNL1/EXP, binds specifically to CHHG repeats. Human
674 molecular genetics 13, 495-507.

675 Kuroyanagi, H., Kobayashi, T., Mitani, S., and Hagiwara, M. (2006). Transgenic
676 alternative-splicing reporters reveal tissue-specific expression profiles and
677 regulation mechanisms in vivo. Nature methods 3, 909-915.

678 Lah, G.J., Li, J.S., and Millard, S.S. (2014). Cell-specific alternative splicing of
679 Drosophila Dscam2 is crucial for proper neuronal wiring. Neuron 83, 1376-1388.

680 Lai, S.L., and Lee, T. (2006). Genetic mosaic with dual binary transcriptional
681 systems in Drosophila. Nature neuroscience 9, 703-709.

682 Lee, T., and Luo, L. (1999). Mosaic analysis with a repressible cell marker for
683 studies of gene function in neuronal morphogenesis. Neuron 22, 451-461.

684 Li, J.S., Shin, G.J., and Millard, S.S. (2015). Neuronal cell-type-specific alternative
685 splicing: A mechanism for specifying connections in the brain? Neurogenesis 2,
686 e1122699.

687 Li, L.B., Yu, Z., Teng, X., and Bonini, N.M. (2008). RNA toxicity is a component of
688 ataxin-3 degeneration in Drosophila. Nature 453, 1107-1111.

689 Llamusi, B., Bargiela, A., Fernandez-Costa, J.M., Garcia-Lopez, A., Klima, R.,
690 Feiguin, F., and Artero, R. (2013). Muscleblind, BSF and TBPH are mislocalized in
691 the muscle sarcomere of a Drosophila myotonic dystrophy model. Disease
692 models & mechanisms 6, 184-196.

693 Machuca-Tzili, L.E., Buxton, S., Thorpe, A., Timson, C.M., Wigmore, P., Luther, P.K.,
694 and Brook, J.D. (2011). Zebrafish deficient for Muscleblind-like 2 exhibit features
695 of myotonic dystrophy. Disease models & mechanisms 4, 381-392.

696 Markovtsov, V., Nikolic, J.M., Goldman, J.A., Turck, C.W., Chou, M.Y., and Black, D.L.
697 (2000). Cooperative assembly of an hnRNP complex induced by a tissue-specific
698 homolog of polypyrimidine tract binding protein. Molecular and cellular biology
699 20, 7463-7479.

700 McKee, A.E., Minet, E., Stern, C., Riahi, S., Stiles, C.D., and Silver, P.A. (2005). A
701 genome-wide in situ hybridization map of RNA-binding proteins reveals
702 anatomically restricted expression in the developing mouse brain. BMC
703 developmental biology 5, 14.

704 Millard, S.S., Flanagan, J.J., Pappu, K.S., Wu, W., and Zipursky, S.L. (2007). Dscam2
705 mediates axonal tiling in the Drosophila visual system. Nature 447, 720-724.

706 Millard, S.S., Lu, Z., Zipursky, S.L., and Meinertzhagen, I.A. (2010). Drosophila
707 dscam proteins regulate postsynaptic specificity at multiple-contact synapses.
708 Neuron 67, 761-768.

709 Mondal, K., VijayRaghavan, K., and Varadarajan, R. (2007). Design and utility of
710 temperature-sensitive Gal4 mutants for conditional gene expression in
711 Drosophila. Fly 1, 282-286.

712 Nern, A., Pfeiffer, B.D., and Rubin, G.M. (2015). Optimized tools for multicolor
713 stochastic labeling reveal diverse stereotyped cell arrangements in the fly visual
714 system. Proceedings of the National Academy of Sciences of the United States of
715 America 112, E2967-E2976.

716 Newsome, T.P., Schmidt, S., Dietzl, G., Keleman, K., Asling, B., Debant, A., and
717 Dickson, B.J. (2000). Trio combines with dock to regulate Pak activity during
718 photoreceptor axon pathfinding in Drosophila. Cell 101, 283-294.

719 Ni, J.Q., Markstein, M., Binari, R., Pfeiffer, B., Liu, L.P., Villalta, C., Booker, M.,
720 Perkins, L., and Perrimon, N. (2008). Vector and parameters for targeted
721 transgenic RNA interference in Drosophila melanogaster. Nature methods 5, 49-
722 51.

723 Nilsen, T.W., and Graveley, B.R. (2010). Expansion of the eukaryotic proteome by
724 alternative splicing. Nature 463, 457-463.

725 Norris, A.D., Gao, S., Norris, M.L., Ray, D., Ramani, A.K., Fraser, A.G., Morris, Q.,
726 Hughes, T.R., Zhen, M., and Calarco, J.A. (2014). A pair of RNA-binding proteins
727 controls networks of splicing events contributing to specialization of neural cell
728 types. Molecular cell 54, 946-959.

729 Norris, A.D., Gracida, X., and Calarco, J.A. (2017). CRISPR-mediated genetic
730 interaction profiling identifies RNA binding proteins controlling metazoan
731 fitness. eLife 6.

732 Ohno, G., Hagiwara, M., and Kuroyanagi, H. (2008). STAR family RNA-binding
733 protein ASD-2 regulates developmental switching of mutually exclusive
734 alternative splicing in vivo. Genes & development 22, 360-374.

735 Pan, Q., Shai, O., Lee, L.J., Frey, B.J., and Blencowe, B.J. (2008). Deep surveying of
736 alternative splicing complexity in the human transcriptome by high-throughput
737 sequencing. Nature genetics 40, 1413-1415.

738 Parks, A.L., Cook, K.R., Belvin, M., Dompe, N.A., Fawcett, R., Huppert, K., Tan, L.R.,
739 Winter, C.G., Bogart, K.P., Deal, J.E., *et al.* (2004). Systematic generation of high-
740 resolution deletion coverage of the Drosophila melanogaster genome. Nature
741 genetics 36, 288-292.

742 Pascual, M., Vicente, M., Monferrer, L., and Artero, R. (2006). The Muscleblind
743 family of proteins: an emerging class of regulators of developmentally
744 programmed alternative splicing. Differentiation; research in biological diversity
745 74, 65-80.

746 Schreiner, D., Nguyen, T.M., Russo, G., Heber, S., Patrignani, A., Ahrne, E., and
747 Scheiffele, P. (2014). Targeted combinatorial alternative splicing generates brain
748 region-specific repertoires of neurexins. Neuron 84, 386-398.

749 Spradling, A.C., Stern, D., Beaton, A., Rhem, E.J., Laverty, T., Mozden, N., Misra, S.,
750 and Rubin, G.M. (1999). The Berkeley Drosophila Genome Project gene
751 disruption project: Single P-element insertions mutating 25% of vital Drosophila
752 genes. Genetics 153, 135-177.

753 Tadros, W., Xu, S.W., Akin, O., Yi, C.H., Shin, G.J.E., Millard, S.S., and Zipursky, S.L.
754 (2016). Dscam Proteins Direct Dendritic Targeting through Adhesion. Neuron
755 89, 480-493.

756 Tan, L., Zhang, K.X., Pecot, M.Y., Nagarkar-Jaiswal, S., Lee, P.T., Takemura, S.Y.,
757 McEwen, J.M., Nern, A., Xu, S., Tadros, W., *et al.* (2015). Ig Superfamily Ligand and
758 Receptor Pairs Expressed in Synaptic Partners in Drosophila. Cell 163, 1756-
759 1769.

760 Tomioka, M., Naito, Y., Kuroyanagi, H., and Iino, Y. (2016). Splicing factors control
761 C. elegans behavioural learning in a single neuron by producing DAF-2c receptor.
762 Nature communications 7, 11645.

763 Underwood, J.G., Boutz, P.L., Dougherty, J.D., Stoilov, P., and Black, D.L. (2005).
764 Homologues of the Caenorhabditis elegans Fox-1 protein are neuronal splicing
765 regulators in mammals. Molecular and cellular biology 25, 10005-10016.

766 Venken, K.J., Schulze, K.L., Haelterman, N.A., Pan, H., He, Y., Evans-Holm, M.,
767 Carlson, J.W., Levis, R.W., Spradling, A.C., Hoskins, R.A., and Bellen, H.J. (2011).
768 MiMIC: a highly versatile transposon insertion resource for engineering
769 Drosophila melanogaster genes. Nature methods 8, 737-743.

770 Vicente, M., Monferrer, L., Poulos, M.G., Houseley, J., Monckton, D.G., O'Dell K, M.,
771 Swanson, M.S., and Artero, R.D. (2007). Muscleblind isoforms are functionally
772 distinct and regulate alpha-actinin splicing. Differentiation; research in biological
773 diversity 75, 427-440.

774 Wang, E.T., Sandberg, R., Luo, S., Khrebtukova, I., Zhang, L., Mayr, C., Kingsmore,
775 S.F., Schroth, G.P., and Burge, C.B. (2008). Alternative isoform regulation in
776 human tissue transcriptomes. Nature 456, 470-476.

Wang, Q., Abruzzi, K.C., Rosbash, M., and Rio, D.C. (2018). Striking circadian neuron diversity and cycling of Drosophila alternative splicing. eLife 7.

Warzecha, C.C., Sato, T.K., Nabet, B., Hogenesch, J.B., and Carstens, R.P. (2009). ESRP1 and ESRP2 are epithelial cell-type-specific regulators of FGFR2 splicing. Molecular cell 33, 591-601.

Xu, T., and Rubin, G.M. (1993). Analysis of genetic mosaics in developing and adult Drosophila tissues. Development 117, 1223-1237.

Li et al. Figure 1.

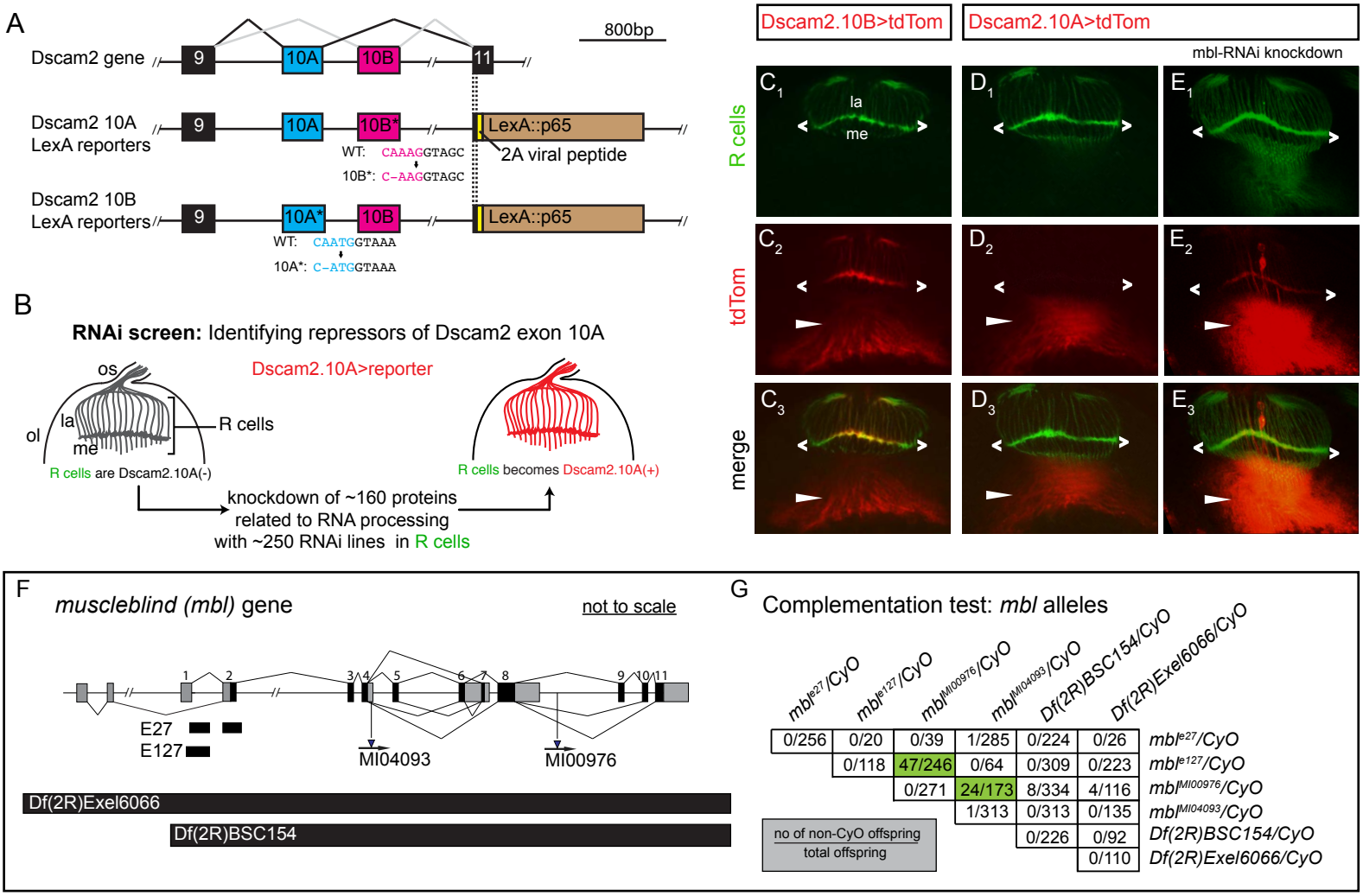

Li et al. Figure 2.

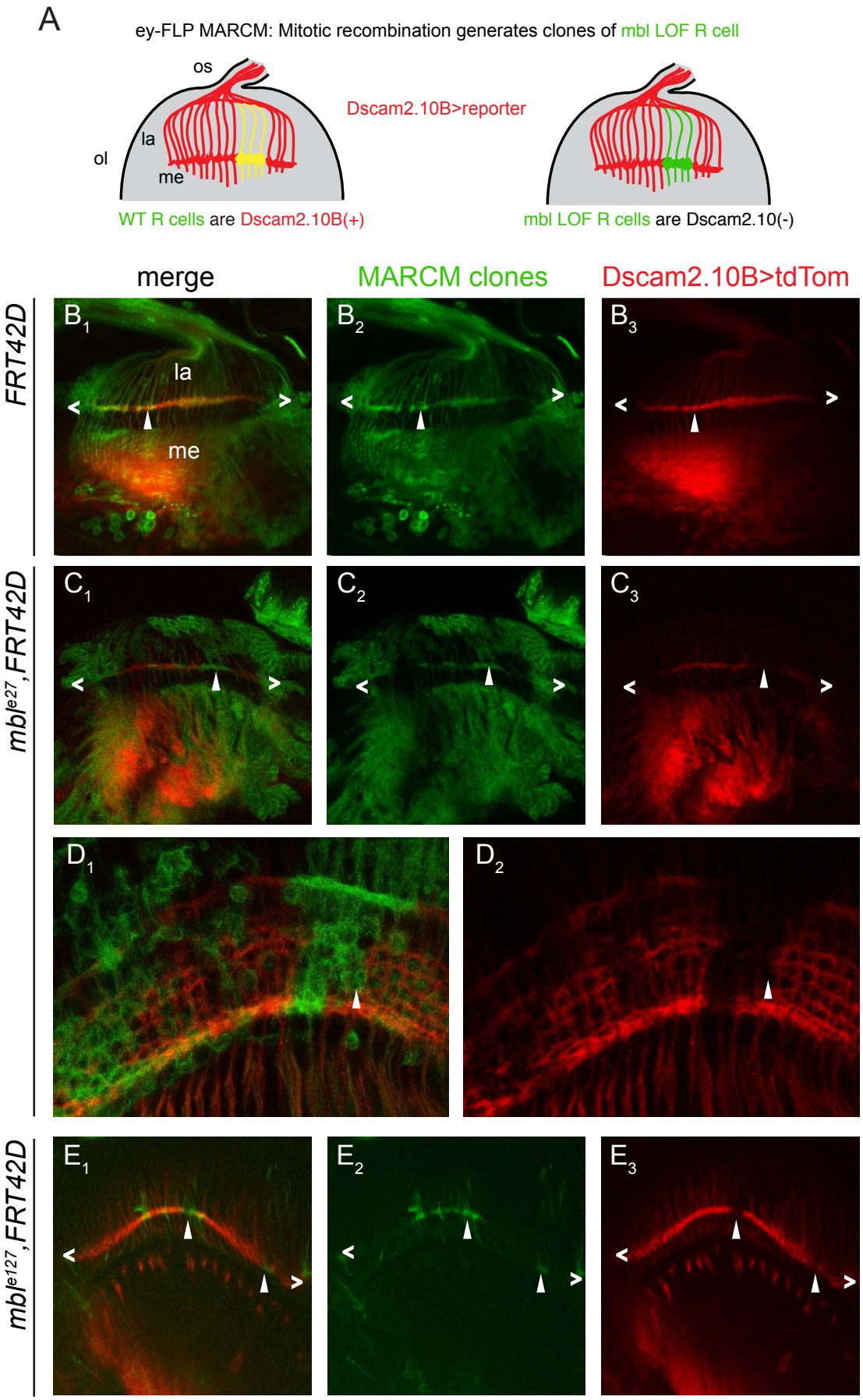

Li et al. Figure 3.

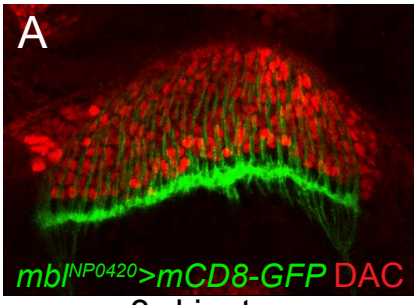

3rd instar

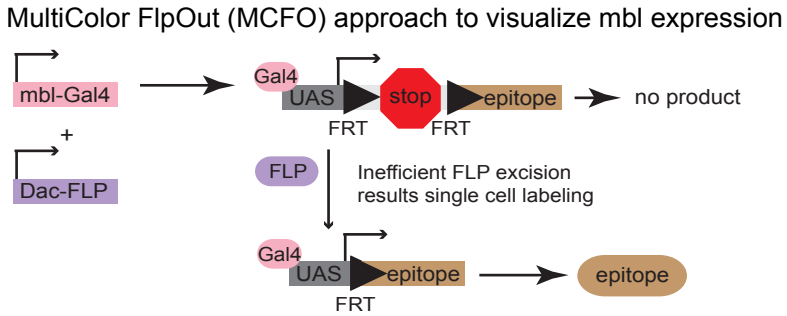

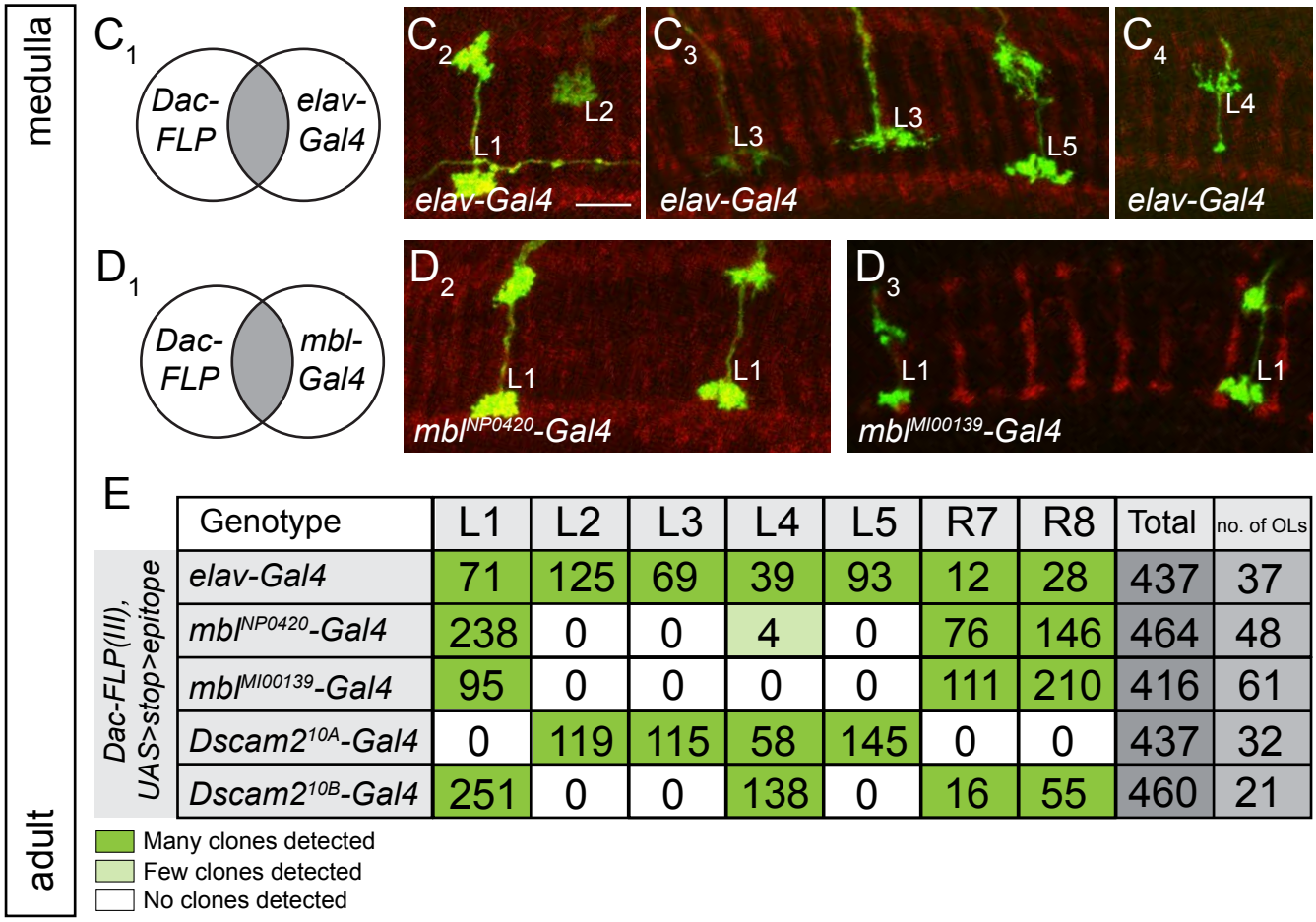

E

	Genotype	L1	L2	L3	L4	L5	R7	R8	Total	no. of OLs
Dac-FLP(III), UAS>stop>epitope	*elav-Gal4*	71	125	69	39	93	12	28	437	37
	mblNP0420-Gal4	238	0	0	4	0	76	146	464	48
	mblMI00139-Gal4	95	0	0	0	0	111	210	416	61
	Dscam2 10A-Gal4	0	119	115	58	145	0	0	437	32
	Dscam2 10B-Gal4	251	0	0	138	0	16	55	460	21

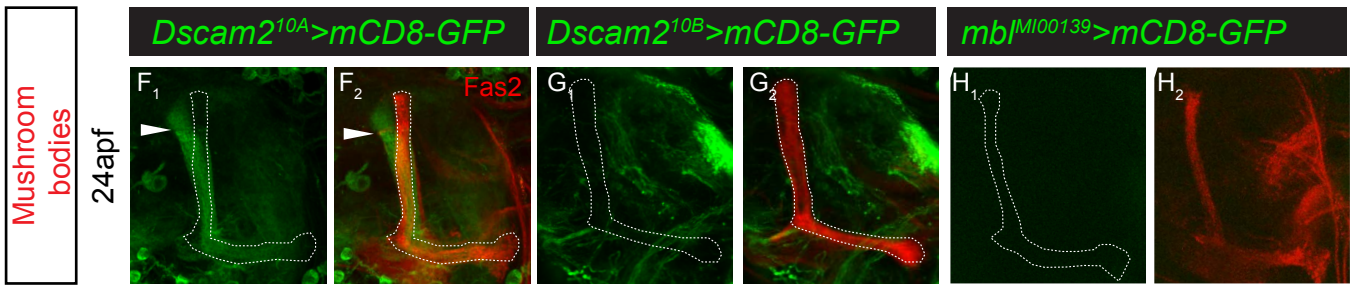

Li et al. Figure 4.

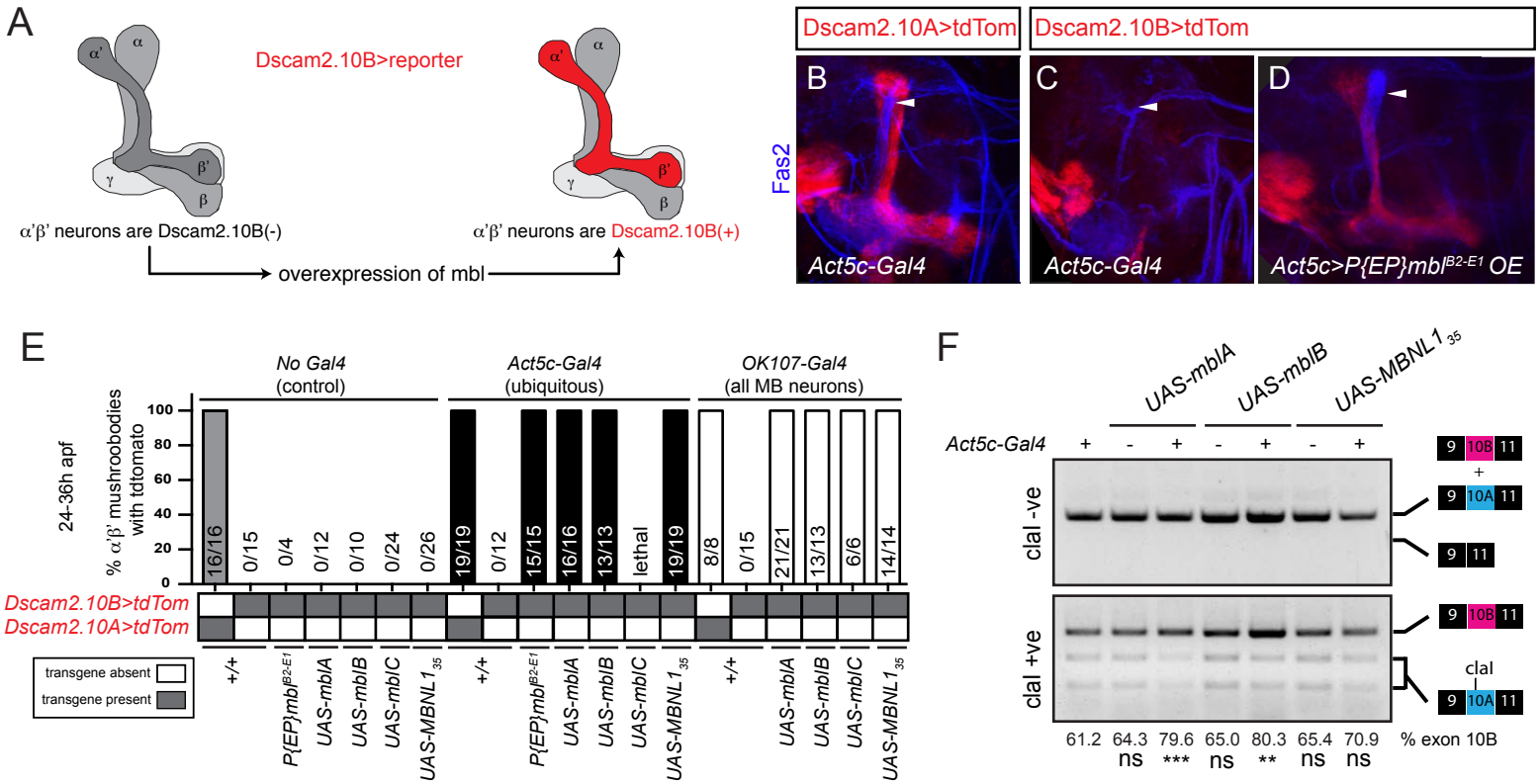

Figure 5.

mbl loss-of-function (LOF)

A

	Genotype		L1	L2	L3	L4	L5	Total	no. of OLs
27G05-FLP(X), UAS>stop>epitope	*Dscam2^{10B}-Gal4*	+/+	359	0	0	118	0	477	11
	Dscam2^{10A}-Gal4	+/+	0	94	105	58	146	403	10
		mbl^{e127}/+	1	96	99	117	147	460	10
		mbl^{MI00976}/+	1	102	114	111	155	483	11
		mbl^{e127}/mbl^{MI00976}	45 #	82	105	120	141	493	10

B

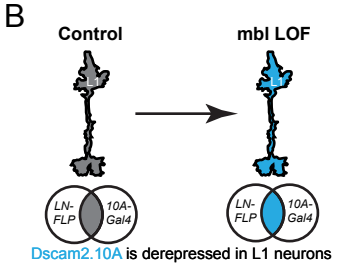

mbl overexpression (OE)

C

	Genotype		L1	L2	L3	L4	L5	Total	no. of OLs
27G05-FLP(X), LexAop>stop>epitope	*Dscam2^{10A}-LexA*	*elav-Gal4*	0	57	63	12	89	221	18
	Dscam2^{10B}-LexA	*elav-Gal4*	117	0	0	70	0	187	20
		elav-Gal4+UAS-mblB	77	65 #	31 #	29	28 #	230	22

D

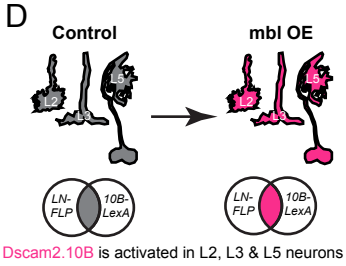

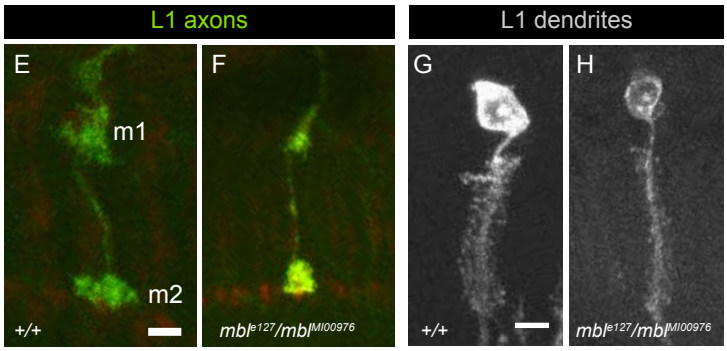

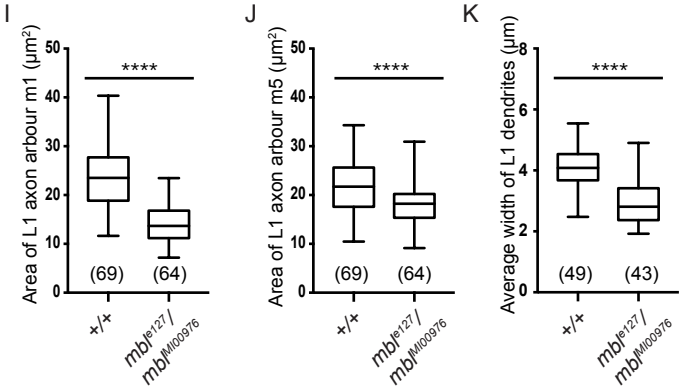

Fly genotypes

R cell RNAi experiments (Figure 1)

1. *w; GMR-GFP, GMR-Gal4/CyO; Dscam2.10B-LexA, LexAop-myr-tdTomato/TM6B*

2. *w; GMR-GFP, GMR-Gal4/CyO; Dscam2.10A-LexA, LexAop-myr-tdTomato/TM6B*

3. *w, UAS-Dcr-2; GMR-GFP, GMR-Gal4/CyO; Dscam2.10A-LexA, LexAop-myr-tdTomato/TM6B*

4. *w, UAS-Dcr-2; GMR-GFP, GMR-Gal4/UAS-mCD8-RFP; Dscam2.10A-LexA, LexAop-myr-tdTomato/+*

5. *w, UAS-Dcr-2; GMR-GFP, GMR-Gal4/UAS-mbl-RNAi(v28732); Dscam2.10A-LexA, LexAop-myr-tdTomato/+*

6. *w, UAS-Dcr-2; GMR-GFP, GMR-Gal4/+; Dscam2.10A-LexA, LexAop-myr-tdTomato/UAS-mbl-RNAi(TRiP.JF03264)*

mbl whole animal experiments (Figure 1)

1. *w; +; Dscam2.10B-LexA, LexAop-myr-tdTomato/TM6B*

2. *w; +; Dscam2.10A-LexA, LexAop-myr-tdTomato/TM6B*

3. *w; mbl^{e127}/CyO,GFP; Dscam2.10A-LexA, LexAop-myr-tdTomato/TM6B*

4. *w; $mbl^{MI00976}$/CyO,GFP; Dscam2.10A-LexA, LexAop-myr-tdTomato/TM6B*

5. *w; $mbl^{MI04093}$/CyO,GFP; Dscam2.10A-LexA, LexAop-myr-tdTomato/TM6B*

6. *w; mbl^{e127}/ $mbl^{MI00976}$; Dscam2.10A-LexA, LexAop-myr-tdTomato/+*

7. *w; $mbl^{MI04093}$/ $mbl^{MI00976}$; Dscam2.10A-LexA, LexAop-myr-tdTomato/+*

mbl ey-FLP MARCM experiments (Figure 2)

1. *w, ey-FLP; FRT42D, Tub-Gal80/FRT42D; Dscam2.10A-LexA, LexAop-myr-tdTomato, Act5c-Gal4, UAS-mCD8-GFP/+*

2. *w, ey-FLP; FRT42D, Tub-Gal80/FRT42D, mbl^{e27}; Dscam2.10A-LexA, LexAop-myr-tdTomato, Act5c-Gal4, UAS-mCD8-GFP/+*

3. *w, ey-FLP; FRT42D, Tub-Gal80/FRT42D, mbl^{e127}; Dscam2.10A-LexA, LexAop-myr-tdTomato, Act5c-Gal4, UAS-mCD8-GFP/+*

<u>mbl expression experiments (Figure 3)</u>

1. *w; UAS-mCD8-GFP/+; mbl^{NP0420}-Gal4/+*

2. *w; UAS-mCD8-GFP/+; mbl^{MI00139}-Gal4/+*

3. *w; Dac-FLP/+; elav-Gal4/ UAS>stop>myr::smGdP-V5-THS-UAS>stop>myr::smGdP-cMyc*

4. *w; Dac-FLP/+; mbl^{NP0420}-Gal4/ UAS>stop>myr::smGdP-V5-THS-UAS>stop>myr::smGdP-cMyc*

5. *w; Dac-FLP/+; mbl^{MI00139}-Gal4/ UAS>stop>myr::smGdP-V5-THS-UAS>stop>myr::smGdP-cMyc*

6. *w; Dac-FLP/+; Dscam2.10A-Gal4/ UAS>stop>myr::smGdP-V5-THS-UAS>stop>myr::smGdP-cMyc*

7. *w; Dac-FLP/+; Dscam2.10B-Gal4/ UAS>stop>myr::smGdP-V5-THS-UAS>stop>myr::smGdP-cMyc*

8. *w; +; mbl^{NP0420}-Gal4/UAS-GFP.nls*

9. *w; +; mbl^{MI00139}-Gal4/UAS-GFP.nls*

<u>mbl ectopic expression in MBs (Figure 4)</u>

1. *w; +; Dscam2.10A-LexA, LexAop-myr-tdTomato, Act5c-Gal4, UAS-mCD8-GFP/+*

2. *w; +; Dscam2.10B-LexA, LexAop-myr-tdTomato, Act5c-Gal4, UAS-mCD8-GFP/+*

3. *w; P{EP}mbl$^{B2\text{-}E1}$/+; Dscam2.10B-LexA, LexAop-myr-tdTomato, Act5c-Gal4, UAS-mCD8-GFP/+*

4. *w; +; Dscam2.10B-LexA, LexAop-myr-tdTomato, Act5c-Gal4, UAS-mCD8-GFP/UAS-mblA*

5. *w; +; Dscam2.10B-LexA, LexAop-myr-tdTomato, Act5c-Gal4, UAS-mCD8-GFP/UAS-mblB*

6. *w; +; Dscam2.10B-LexA, LexAop-myr-tdTomato, Act5c-Gal4, UAS-mCD8-GFP/UAS-mblC*

7. *w; +; Dscam2.10B-LexA, LexAop-myr-tdTomato, Act5c-Gal4,UAS-mCD8-GFP/UAS-MBNL1$_{35}$*

8. *w; +; Dscam2.10B-LexA, LexAop-myr-tdTomato, UAS-mCD8-GFP/UAS-mblA; OK107-Gal4/+*

9. *w; +; Dscam2.10B-LexA, LexAop-myr-tdTomato, UAS-mCD8-GFP/UAS-mblB; OK107-Gal4/+*

10. *w; +; Dscam2.10B-LexA, LexAop-myr-tdTomato, UAS-mCD8-GFP/UAS-mblC; OK107-Gal4/+*

11. *w; +; Dscam2.10B-LexA, LexAop-myr-tdTomato, UAS-mCD8-GFP/UAS-MBNL1$_{35}$; OK107-Gal4/+*

<u>Lamin neuron FlpOut mbl LOF (Figure 5)</u>

1. *w, 27G05-FLP/(+ or Y); Bl/CyO; Dscam2.10B-Gal4/ UAS>stop>myr::smGdP-V5-THS-UAS>stop>myr::smGdP-cMyc*

2. *w, 27G05-FLP/(+ or Y); Bl/CyO; Dscam2.10A-Gal4/ UAS>stop>myr::smGdP-V5-THS-UAS>stop>myr::smGdP-cMyc*

3. *w, 27G05-FLP/(+ or Y); mbl^{e127}/ CyO; Dscam2.10A-Gal4/ UAS>stop>myr::smGdP-V5-THS-UAS>stop>myr::smGdP-cMyc*

4. *w, 27G05-FLP/(+ or Y); mbl^{MI00976}/CyO; Dscam2.10A-Gal4/ UAS>stop>myr::smGdP-V5-THS-UAS>stop>myr::smGdP-cMyc*

5. *w, 27G05-FLP/(+ or Y); mbl^{e127}/ mbl^{MI00976}; Dscam2.10A-Gal4/ UAS>stop>myr::smGdP-V5-THS-UAS>stop>myr::smGdP-cMyc.*

6. *w, 27G05-FLP/(+ or Y); elav-Gal4/LexAop2>stop>myr::smGdP-V5; Dscam2.10A-LexA/TM2.*

7. *w, 27G05-FLP/(+ or Y); elav-Gal4/LexAop2>stop>myr::smGdP-V5; Dscam2.10B-LexA/TM2.*

8. *w, 27G05-FLP/(+ or Y); elav-Gal4/LexAop2>stop>myr::smGdP-V5; Dscam2.10B-LexA/UAS-mblB.*

<u>L1 axonal and dendritic defects (Figure 5)</u>

1. *w, 27G05-FLP/(+ or Y); Bl.CyO; Dscam2.10A-Gal4/ UAS>stop>myr::smGdP-V5-THS-UAS>stop>myr::smGdP-cMyc.*

2. *w, 27G05-FLP/(+ or Y); mbl^{e127}/ mbl^{MI00976}; Dscam2.10A-Gal4/ UAS>stop>myr::smGdP-V5-THS-UAS>stop>myr::smGdP-cMyc.*

<u>mbl ey-FLP mosaic experiments (Figure S1)</u>

1. *w, ey-FLP; FRT42D, GMR-myr-GFP/FRT42D; Dscam2.10B-LexA, LexAop-myr-tdTomato, UAS-mCD8-GFP/+*

2. *w, ey-FLP; FRT42D, GMR-myr-GFP/FRT42D; Dscam2.10A-LexA, LexAop-myr-tdTomato, UAS-mCD8-GFP/+*

3. *w, ey-FLP; FRT42D, GMR-myr-GFP/FRT42D, Df(2R)154 ; Dscam2.10A-LexA, LexAop-myr-tdTomato, UAS-mCD8-GFP/+*

4. *w, ey-FLP; FRT42D, GMR-myr-GFP/FRT42D, mbl^{e27}; Dscam2.10A-LexA, LexAop-myr-tdTomato, UAS-mCD8-GFP/+*

5. *w, ey-FLP; FRT42D, GMR-myr-GFP/FRT42D, mbl^{MI00976}; Dscam2.10A-LexA, LexAop-myr-tdTomato, UAS-mCD8-GFP/+*

<u>*mbl* expression (Figure S3)</u>

1. *w; mbl^{K01212}-LacZ*

2. *w; mbl^{NP1161}-Gal4/CyO, UAS-LacZ*

3. *w; mbl^{MI00139}-Gal4/+; UAS-CD8-GFP/+*

4. *w; mbl^{MI00139}-Gal4/UAS-GFP.nls*

5. *w; mbl^{NP0420}-Gal4/UAS-GFP.nls*

<u>MB axon defects (Figure S5)</u>

1. *w; +; +*

2. *w; +; Dscam2^{null}/ Dscam2^{null}*

3. *w; +; Dscam2A/ Dscam2A*

4. *w; +; Dscam2B/ Dscam2B*

5. *w; mbl^{e127}/ mbl^{MI00976}*

6. *w; +; +; OK107-Gal4/+*

7. *w; UAS-mbl-RNAi(v28732)/+*

8. *w; UAS-mbl-RNAi(v28732)/+; +; OK107-Gal4/+*

9. *w; P{EP}mbl^{B2-E1}/+*

10. *w; P{EP}mbl^{B2-E1}/+; +; OK107-Gal4/+*

11. *w; +; UAS-mblA/+*

12. *w; +; UAS-mblA/+; OK107-Gal4/+*

13. *w; +; UAS-mblB/+*

14. *w; +; UAS-mblB/+; OK107-Gal4/+*

15. *w; +; UAS-mblC/+*

16. *w; +; UAS-mblC/+; OK107-Gal4/+*

17. *w; +; UAS-MBNL1*$_{35}$*/+*

18. *w; +; UAS-MBNL1*$_{35}$*/+; OK107-Gal4/+*

Figure S1. Related to Figure 1. *Mbl* LOF results in aberrant *Dscam2*.10A reporter expression in eye mosaic clones.

(A-F) Eye mosaics of *mbl* LOF alleles cause de-repression of *Dscam2.10A>tdTom* in R cells. *WT* mosaic clones (GFP-negative) express *Dscam2.10B>tdTom* (A_1-A_4) but not *Dscam2.10A>tdTom* (B_1-B_4). *Mbl* mutant (GFP-negative) clones, *Df(2R)BSC154* show aberrant *Dscam2.10A* expression in R cells (C_1-C_4). (D) mbl^{e27} eye clones exhibit de-repression of Dscam2.10A (red). (E) Clones of a *mbl* allele that deleted only a portion of all mbl isoforms ($mbl^{MI00976}$) do not exhibit de-repression of Dscam2.10A. (F) Quantification of *Dscam2.10>tdTom* expression in third instar R cells with *mbl* LOF eye mosaic clones. Y-axis represents the number of optic lobes with R cells positive for tdTom over total number of optic lobes quantified as a percentage. On the x-axis, the presence of a transgene is indicated with a grey box.

Figure S2. Related to Figure 1. *Mbl* LOF is associated with increased *Dscam2.10A* inclusion without affecting other *Dscam2* splicing events.

(A) *Mbl* LOF ($mbl^{e127}/mbl^{MI00976}$) does not affect other *Dscam2* splicing events. Semiquantitative RT-PCR from different genotypes indicated. Primers amplified the variable region that includes exon 19S/19L or three alternative last exons (ALE). Percentage of 19L inclusion was calculated by dividing the 19L band by 19L+19S. Percentage of ALE 21A and ALE 21BL inclusion was calculated by dividing respectively the 21A and 21BL band by 21A+21BL+21BS (total). (B) Graphs of RT-PCR data from A and Figure 1P. Top graph depicts Dscam2.10A inclusion. Middle graph represents exon 19S inclusion. Bottom graph represents percentage inclusion of different ALEs. Plots show minimum (bottom line), mean (middle line) and maximum (top line) points, where individual points depict biological replicates.

Dashed line represents mean of control. (C) Quantitative RT-PCR of *mbl* LOF mutant ($mbl^{e127}/mbl^{MI00976}$) show increased exon 10A inclusion and decreased exon 10B inclusion. The left graph shows *Dscam2.10* levels compared to *synaptobrevin* (*nSyb*). The middle graph shows *Dscam2.10A* levels compared to *Dscam2.10*. The right graph shows *Dscam2.10B* levels compared to *Dscam2*. Bar graph format (error bars depict standard error of means). The y-axis is the relative quantity (Rq). Dashed line represents mean of control. Unpaired t-test was conducted to compare Rq levels between control and *mbl* LOF mutants. ns $P > 0.05$, * $P < 0.05$, ** $P < 0.01$.

Figure S3. Related to Figure 3. *Mbl* is expressed in R cells, neurons and glia

(A) Schematic showing the insertion locations of different *mbl* reporters. Translated regions (black) and non-translated regions (grey) are shown.

(B-D) *Mbl* is expressed in R cells (red) in third instar eye-discs (ed). The *mbl* enhancer traps mbl^{K01212}-*LacZ* (B), mbl^{NP1161}-*Gal4* (C) and splicing trap reporter $mbl^{MI00139}$-*Gal4* (D, green*)* overlapped with a marker of R cells (24B10).

(E-I) $mbl^{MI00139}$>*GFP.nls* is expressed in neurons and muscles. (E_1-E_2) Representative confocal image of a $mbl^{MI00139}$>*GFP.nls* (green) adult brain co-labelled with an ELAV antibody (red). Dashed lines demarcate GFP(+) cells. Yellow solid arrowheads show GFP(+) cells that are ELAV(-). (F) Quantification of *mbl* in third instar and adult brains where ~90-100% of GFP(+) cells are also ELAV(+) (black bars). Y-axis represents the number of GFP(+) cells positive for ELAV quantified as a percentage. (G_1-G_2) Representative confocal image of a $mbl^{MI00139}$>*GFP.nls* adult brain labelled with a Repo antibody (red). Dashed lines demarcate GFP(+) cells. White solid arrowheads show GFP(+) cells that are positive for Repo. (H) Quantification of $mbl^{MI00139}$>*GFP.nls* where ~0-10% of $mbl^{MI00139}$>*GFP.nls* (+) cells are also

Repo(+).Y-axis represents the number of GFP(+) cells positive for Repo quantified as a percentage. (I_1-I_2) *mbl*^{MI00139}>*GFP.nls* expression is also found in third instar muscles m4-m8, m12 and m13 (Phalloidin, red).

(J_1-J_2) Representative confocal image of a *mbl*^{NP0420}>*GFP.nls* (green) adult brain co-labelled with an ELAV antibody (red). Dashed lines demarcate GFP(+) cells. (K) Quantification of *mbl*^{NP0420}>*GFP.nls* in third instar and adult brains where ~80-90% of GFP(+) cells are also ELAV(+). (L-M) In third instar and adult brains, *mbl*^{NP0420}>*GFP.nls* overlaps minimally with Repo (red). (L_1-L_2) Representative confocal image of a *mbl*^{NP0420}>*GFP.nls* adult brain labelled with Repo. Dashed lines demarcate GFP(+) cells. White solid arrowheads show GFP(+) cells that are positive for Repo. (M) Quantification of *mbl*^{NP0420}>*GFP.nls* in third instar and adult brains where ~10-15% of GFP (+) cells are also Repo(+). (N_1-N_2) *mbl*^{NP0420}>*GFP.nls* expression is not detected in third instar muscles m4-m8, m12 and m13 (Phalloidin, red).

Figure S4. Related to Figure 3. *Mbl* expression is cell-type-specific and correlates with *Dscam2.10B*.

(A) Quantification of lamina neurons and R7-R8 neurons observed using the intersectional strategy during development. Two different *mbl* reporters were used. The transcriptional reporter labelled L4 cells early in development whereas the splicing trap reporter did not. This is most likely due to the lower efficiency of the splicing trap given that it produced 5X fewer L1 clones at 72hr compared to the transcriptional reporter. Green boxes represent detection of reporter expression at different hours after pupal formation (apf). (B) A plot of the percentage of L4 lamina

neurons over total lamina neurons during development (data from the *mbl* transcriptional reporter).

(C-E) *Mbl* is not detected in MB neurons that express *Dscam2.10A* in adults. (C_1-C_2) *Dscam2.10A* is expressed in α'β' mushroom body neurons (asterisks) but not the αβ and g subsets of MB neurons labelled by Fas2 (red). Neither *Dscam2.10B* (D_1-D_2) nor *mbl* (E_1-E_2) are expressed in MB neurons. Neurons in the midline express both *Dscam2.10B* and *mbl* (white arrowhead).

Figure S5. Related to Figure 4. Neurons overexpressing *mbl* phenocopy *Dscam2* single isoform mutants

(A-B) MBs overexpressing *mbl* exhibit defects associated with *Dscam2* single isoform mutants. (A) A representative confocal image of control adult αβ lobes (red) with clear separation between the two β-lobes at the midline. (B) A representative confocal image of adult αβ lobes from an animal overexpressing *mblA*. b-lobe axons inappropriately cross the midline (arrowhead). (C) Quantification of β-lobe axon midline crossing defects. Numbers in parentheses represent total number of MBs quantified. Fishers exact test was used to compare genotypes to their corresponding controls (white bars). ns (not significant) $P>0.05$, * $P<0.05$ and **** $P<0.0001$.

Table S1. Related to Figure 1. List of tested RNAi that did not de-repress Dscam2.10A in R cells

Li et al. Figure S1.

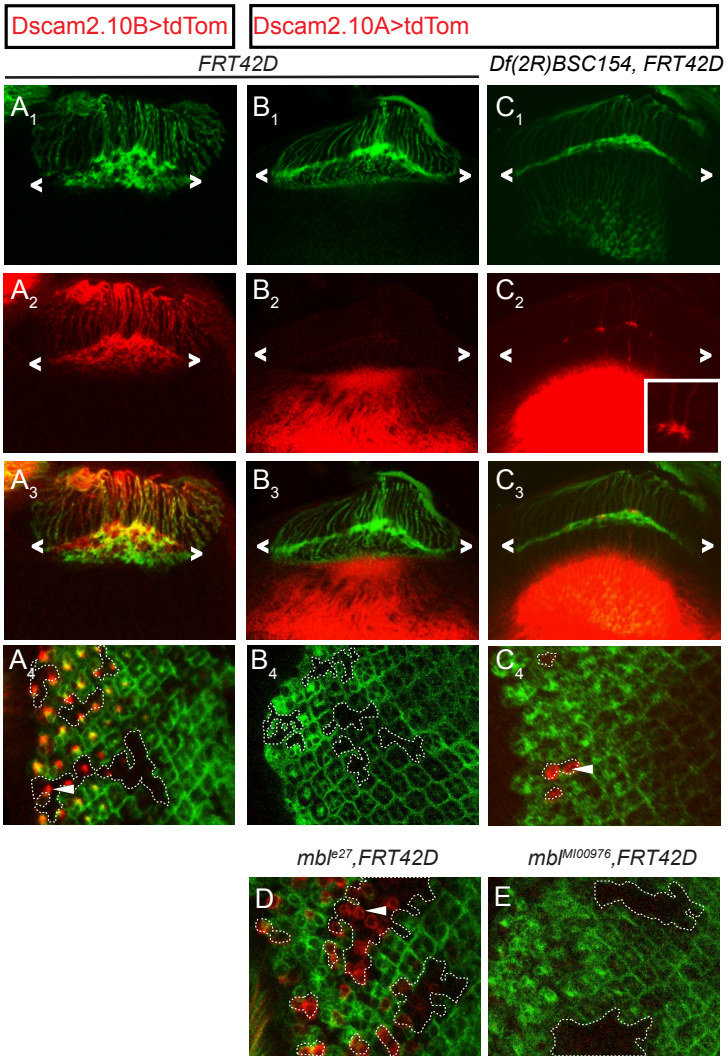

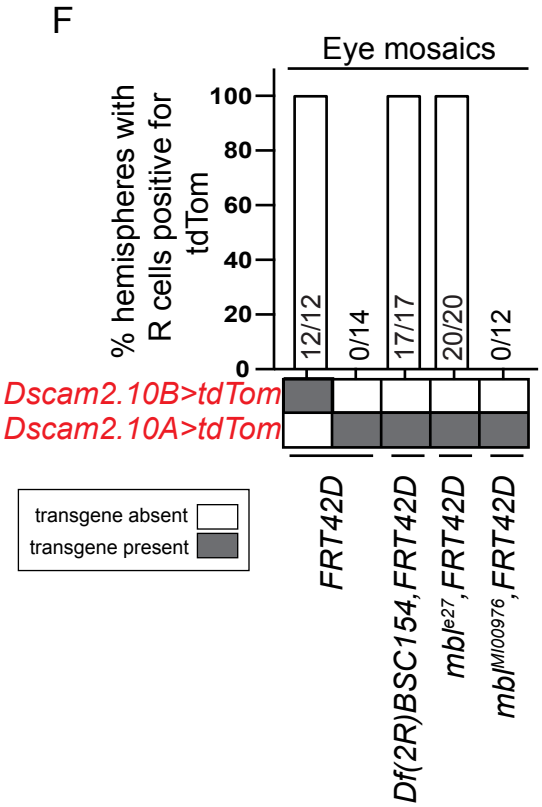

Li et al. Figure S2.

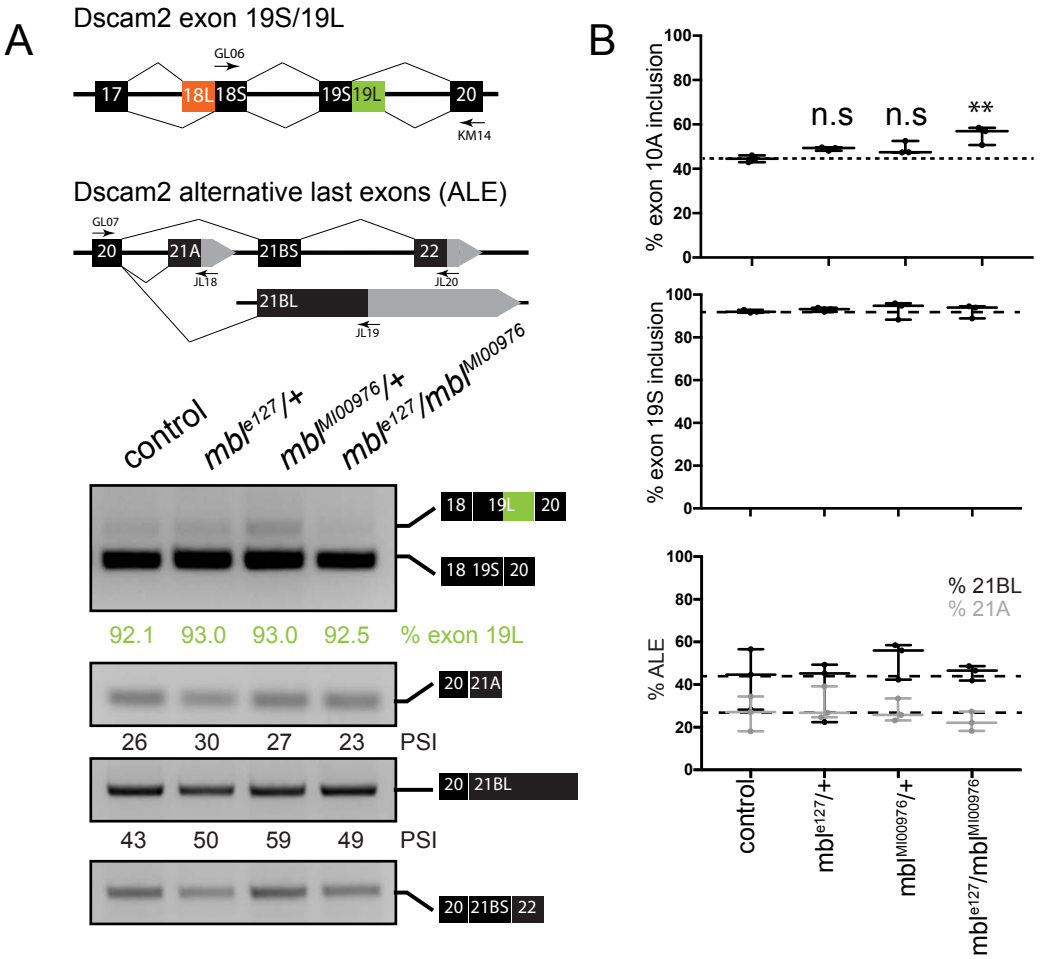

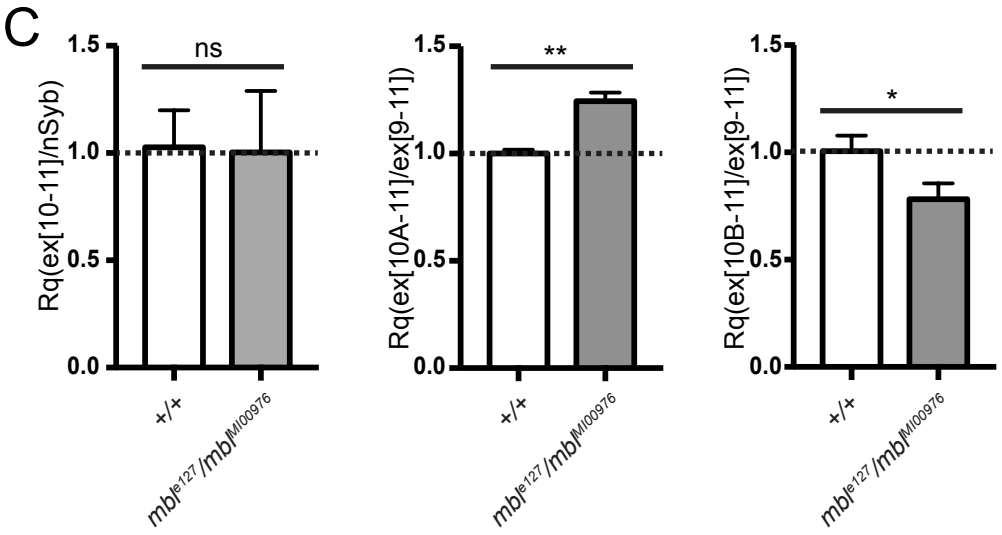

Li et al. Figure S3.

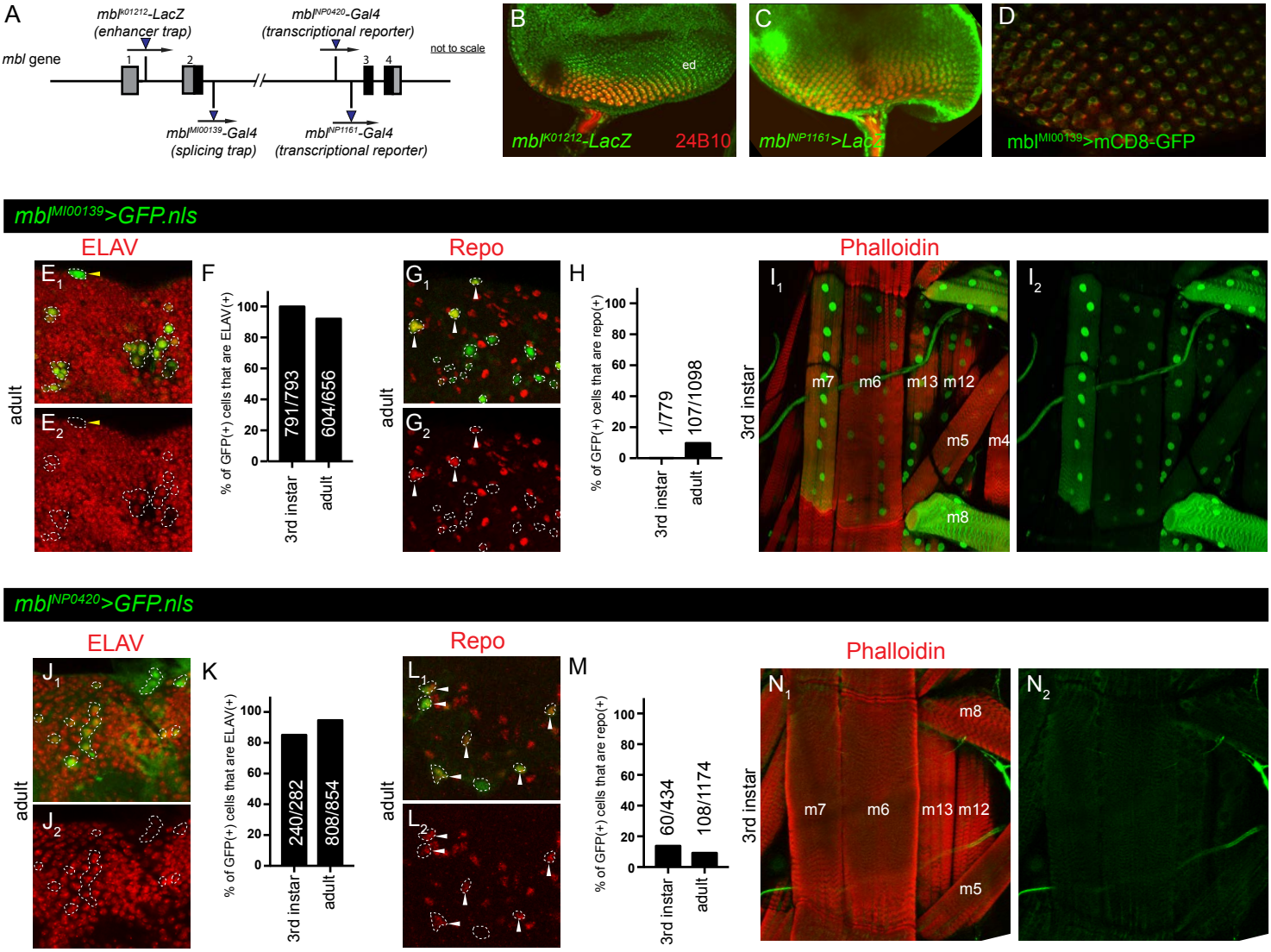

Li et al. Figure S4.

A

Genotype			L1	L2	L3	L4	L5	R7	R8	Total	no. of OLs
Dac-FLP(III), UAS>stop>epitope	*mbl^{NP0420}-Gal4*	72 apf	75	0	0	10	0	10	38	133	8
		60 apf	22	0	0	8	0	15	29	74	8
		48 apf	7	0	0	3	0	1	9	20	2
	mbl^{MI00139}-Gal4	72 apf	15	0	0	0	0	6	15	36	8
		48 apf	12	0	0	0	0	4	24	40	8

Clones detected
No clones detected

B

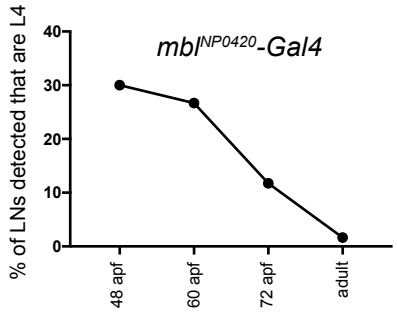

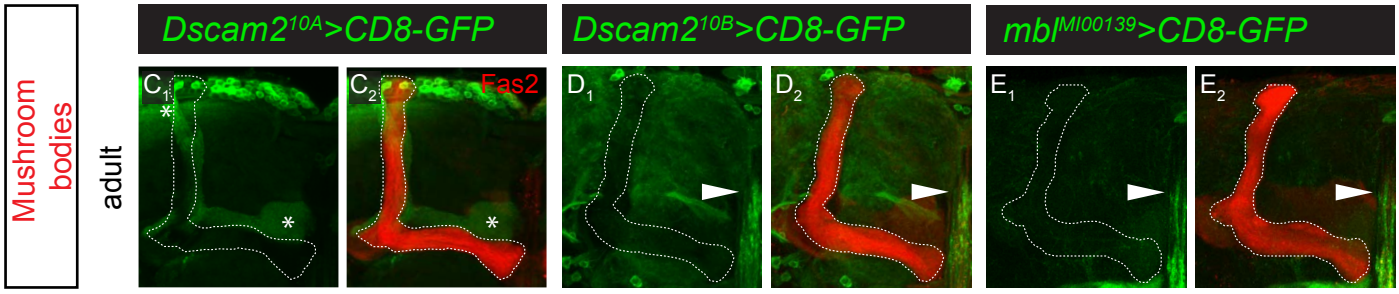

Li et al. Figure S5.

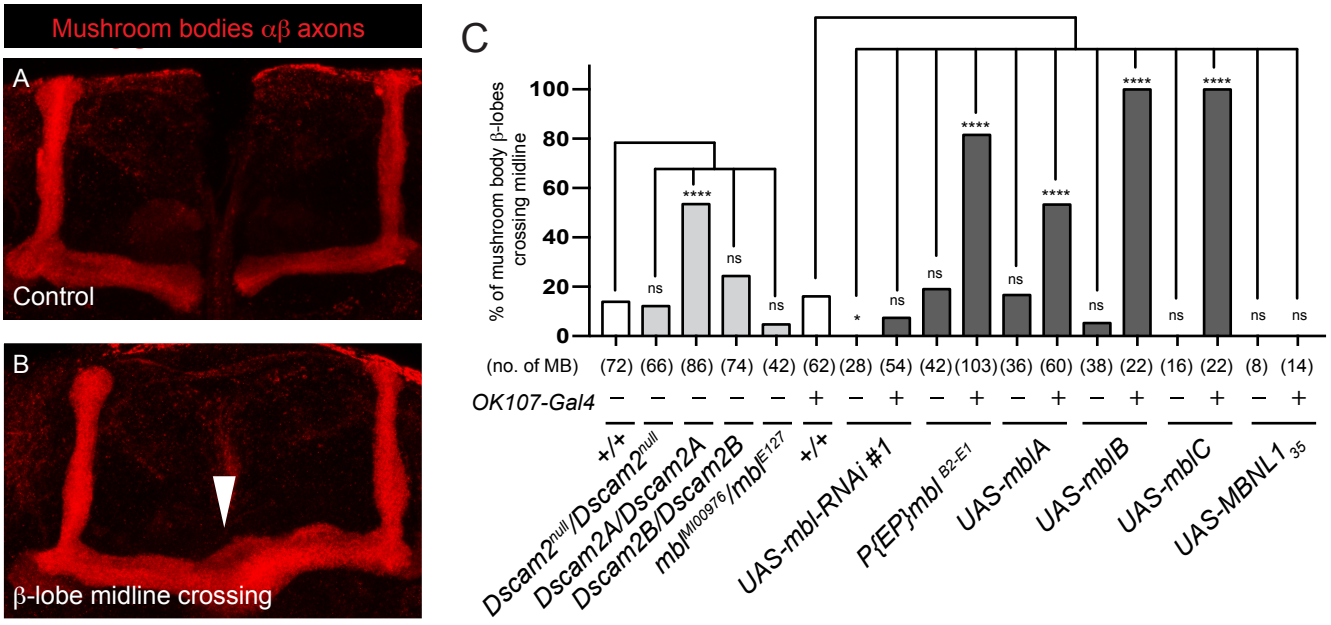

Table S1. List of tested RNAi that did not de-repress Dscam2 exon 10A in R cells

Flybase Number	CG Number	Gene Name	RNAi ID	no. of ol/ed	no. of animals
FBgn0052062	CG32062	A2bp1	27286	12	6
FBgn026239	CG6671	AGO1	33727	3	2
FBgn0000114	CG31762	aret	44483	18	9
FBgn0004587	CG10851	B52	v38862	16	8
FBgn0004587	CG10851	B52	v38860	4	2
FBgn0037660	CG18005	beag	v103832	8	4
FBgn0015907	CG13425	bl	v2912	10	6
FBgn0015907	CG13425	bl	v105271	9	5
FBgn0262475	CG6319	bru-2	50631	13	7
FBgn0264001	CG43744	Bru-3	50734	8	4
FBgn0031883	CG11266	Caper	55742	10	6
FBgn0031883	CG11266	Caper	55742	8	4
FBgn0022942	CG7035	Cbp80	v22331	12	8
FBgn0035136	CG6905	Cdc5	v13492	2	1
FBgn0035136	CG6905	Cdc5	v109369	10	5
FBgn0032690	CG10333	CG10333	v18132	12	8
FBgn0032690	CG10333	CG10333	v18133	4	2
FBgn0036277	CG10418	CG10418	v105940	11	6
FBgn0037531	CG10445	CG10445	v104753	14	7
FBgn0036314	CG10754	CG10754	v31346	11	8
FBgn0039920	CG11360	CG11360	v38491	15	8
FBgn0039920	CG11360	CG11360	v38492	11	6
FBgn0035692	CG13298	CG13298	55257	8	4
FBgn0035162	CG13900	CG13900	v18955	9	6
FBgn0035163	CG13900	CG13900	v108248	16	8
FBgn0037220	CG14641	CG14641	v110507/CyOtb	11	6
FBgn0038464	CG16941	CG16941	v20338	1	1
FBgn0033089	CG17266	CG17266	v25243	10	5
FBgn0033089	CG17266	CG17266	v25244	2	1
FBgn0029751	CG17764	CG17764	v20541	12	7
FBgn0029751	CG17764	CG17764	v101894	10	5
FBgn0035271	CG2021	CG2021	28579	8	5
FBgn0031266	CG2807	CG2807	v25162	8	5
FBgn0037344	CG2926	CG2926	v33589	11	5
FBgn050122	CG30122	CG30122	55209	6	3
FBgn0031631	CG3225	CG3225	v24725	9	5
FBgn0052533	CG32533	CG32533	v38634	1	1
FBgn0052533	CG32533	CG32533	v51785	11	6
FBgn0031628	CG3294	CG3294	v26111/TM6B	12	6
FBgn0031628	CG3294	CG3294	v26111/TM6B	12	6
FBgn0053108	CG33108	CG33108	v24996	9	5
FBgn0031229	CG3436	CG3436	55207/CyOtb	4	2
FBgn0031492	CG3542	CG3542	v26227	10	5
FBgn0031492	CG3542	CG3542	v26229	4	2
FBgn0031493	CG3605	CG3605	v26250	12	7
FBgn0031493	CG3605	CG3605	v26252	8	5
FBgn0035987	CG3689	CG3689	v45278	10	5
FBgn0028474	CG4119	CG4119	v26395	9	5
FBgn0028474	CG4119	CG4119	v106696/CyOtb	10	6
FBgn0034598	CG4266	CG4266	v26472	14	7
FBgn0034598	CG4266	CG4266	v26475	4	2
FBgn0031287	CG4291	CG4291	v21819/TM6B	11	6
FBgn0035016	CG4612	CG4612	v52497	9	5
FBgn0039566	CG4849	CG4849	v21962	9	5
FBgn0032194	CG4901	CG4901	v34904	11	6
FBgn0038344	CG5205	CG5205	v107282	9	5
FBgn0039182	CG5728	CG5728	v24697	14	7
FBgn0038927	CG6015	CG6015	34565	lethal	
FBgn0030631	CG6227	CG6227	v40351	11	8
FBgn0030632	CG6227	CG6227	v40352	12	6
FBgn0004903	CG6354	CG6354	31333	12	9
FBgn0004903	CG6354	CG6354	55662	8	4
FBgn0035675	CG6610	CG6610	v106830	10	6
FBgn0035675	CG6610	CG6610	31870	10	6
FBgn0036828	CG6841	CG6841	v34253/CyOtb	10	5
FBgn0030085	CG6999	CG6999	v110143	11	7
FBgn0030085	CG6999	CG6999	55157	12	6
FBgn0035872	CG7185	CG7185	v107147	5	3
FBgn0035872	CG7185	CG7185	34804	14	7
FBgn0036734	CG7564	CG7564	v100562	10	5
FBgn0035235	CG7879	CG7879	56930	10	5
FBgn0038887	CG7907	CG7907	55370	6	3
FBgn0035253	CG7971	CG7971	v101384	10	7
FBgn0027567	CG8108	CG8108	v35344	12	7
FBgn0030697	CG8565	CG8565	v100449	10	7
FBgn0030697	CG8565	CG8565	55368	11	6
FBgn0032883	CG9323	CG9323	v44984	12	8
FBgn0032883	CG9323	CG9323	v110410	8	4
FBgn0015621	CG3642	Clp	v26259	12	7
FBgn0015621	CG3642	Clp	v26261	13	7
FBgn0263995	CG43738	cpo	28360	8	4
FBgn0027873	CG1957	Cpsf100	50893/TM6B	8	5
FBgn0027873	CG1957	Cpsf100	50893/TM6B	8	5
FBgn0024698	CG10110	Cpsf160	v18009	11	6
FBgn0024698	CG10110	Cpsf160	v110571	9	6
FBgn0261065	CG7698	Cpsf73	v39558	9	5
FBgn0000377	CG3193	crn	v25919	lethal	
FBgn0039867	CG2261	CstF-50	v43716	10	5
FBgn0039867	CG2261	CstF-50	v109583	8	4
FBgn0027841	CG7697	CstF-64	v21045/CyOtb	10	6
FBgn0010220	CG12759	Dbp45A	v17306	6	3
FBgn0010221	CG12760	Dbp45A	v104183	13	7
FBgn0033160	CG11107	Dhx15	v44119/CyOtb	10	6
FBgn0031601	CG3058	Dim1	v21258	10	5
FBgn0259220	CG42320	Doa	v19066	9	5
FBgn0020306	CG9696	dom	v7787	2	1
FBgn0000562	CG4051	egl	28969	8	4
FBgn0001942	CG9075	eIF-4a	v42202	lethal	
FBgn0034237	CG4878	eIF3-S9	32880	lethal	
FBgn0260400	CG4262	elav	28371	2	1
FBgn0033859	CG6197	fand	v104186	10	5
FBgn0036850	CG10419	Gem2	v47372	13	8
FBgn0036850	CG10419	Gem2	v47374	10	7
FBgn0259139	CG6946	glo	33668	9	6
FBgn0259139	CG6946	glo	v27752	12	6
FBgn0001179	CG8019	hay	v41023	12	8
FBgn0014189	CG7269	Hel25E	v22557	9	5
FBgn0011224	CG31000	heph	v33735	10	6
FBgn0011224	CG31000	heph	v110749	18	10
FBgn0264491	CG10293	how	v13756	13	7
FBgn0264491	CG10293	how	v100775	10	5
FBgn0004838	CG10377	Hrb27c, Hrp48	v16040	12	7
FBgn0004838	CG10377	Hrb27c, Hrp48	31685	6	3
FBgn0004838	CG10377	Hrb27c, Hrp48	33716	8	4
FBgn0004237	CG12749	Hrb87F, hrp36	v51759	9	6
FBgn0004237	CG12749	Hrb87F, hrp36	52937	11	6
FBgn0004237	CG12749	Hrb87F, hrp36	31244	14	8
FBgn0001215	CG9983	Hrb98DE, hrp38	31303	10	7
FBgn0001215	CG9983	Hrb98DE, hrp38	32351	13	8
FBgn0015949	CG9854	hrg	v42283	12	6
FBgn0002431	CG9484	hyd	v44675	12	6
FBgn0039691	CG1972	IntS11	v33450	7	5
FBgn0039691	CG1972	IntS11	v109408	8	5
FBgn0036570	CG5222	IntS9	v110367	10	5
FBgn0026713	CG32604	l(1)G0007	v31908	15	8
FBgn0026714	CG32605	l(1)G0008	v31909	4	2
FBgn0086444	CG10689	l(2)37Cb	v31324	9	6
FBgn0263599	CG5931	l(3)72Ab	v43962	5	3
FBgn0263600	CG5932	l(3)72Ab	v110666	6	3
FBgn0035838	CG7942	ldbr	v110582	8	5
FBgn0035838	CG7942	ldbr	55661	8	6
FBgn0034834	CG3162	LS2	v21379	11	7
FBgn0034834	CG3162	LS2	v21380	14	7
FBgn0261067	CG4279	LSm1	v28793	11	6
FBgn0261067	CG4279	LSm1	v50653	10	5
FBgn0033450	CG12924	Lsm11	v108336	12	6
FBgn0051184	CG31184	LSm3	56892	4	2
FBgn0261068	CG13277	Lsm7	v23862	10	6
FBgn0011666	CG5099	msi	55152	10	5
FBgn0262737	CG7437	mub	v28024	16	9
FBgn0014366	CG2925	noi	v20943	9	5
FBgn0015520	CG10328	nonA-I	v101567	7	4
FBgn0015520	CG10328	nonA-I	52934	3	2
FBgn0261619	CG5119	pAbp	v22007	9	5
FBgn0005648	CG2163	Pabp2	v106466	10	5
FBgn0086895	CG8241	pea	v47782	9	5
FBgn0027784	CG6011	Prp18	v13760	10	6
FBgn0027784	CG6011	Prp18	v100287	2	1
FBgn0261119	CG5519	Prp19	v108575	11	6
FBgn0261119	CG5519	Prp19	v41438	3	2
FBgn0036915	CG7757	Prp3	v25548	9	6
FBgn0036487	CG6876	Prp31	v35131	3	2
FBgn0036487	CG6876	Prp31	v103721	6	3
FBgn0033688	CG8877	Prp8	v18565	12	7
FBgn0261552	CG42670	Ps	v44710	18	9
FBgn0261552	CG42670	Ps	v24214	10	5
FBgn0014870	CG8912	Psi	v28989	16	8
FBgn0014870	CG8912	Psi	v28990	10	5
FBgn0014870	CG8912	Psi	v105135	10	7
FBgn0028577	CG12085	pUf68	v109796	8	4
FBgn0003165	CG9755	pum	36676	12	7
FBgn0022987	CG4816	qkr54B	34896	10	5
FBgn0022986	CG3613	qkr58E-1	55159	10	5
FBgn0022985	CG5821	qkr58E-2	55279/CyOtb	6	3
FBgn0022984	CG3584	qkr58E-3	55922	10	5
FBgn0260944	CG17136	Rbp1	v21083/TM6B	12	6
FBgn0260944	CG17136	Rbp1	v110008	11	6
FBgn0030479	CG1987	Rbp1-like	v105883	10	6
FBgn0030479	CG1987	Rbp1-like	44100	4	2
FBgn0260943	CG32169	rbp6	61324/CyOtb	8	4
FBgn0015778	CG9412	rin	33392/TM6B	12	7
FBgn0003261	CG10279	Rm62	v46908/TM6B	12	6
FBgn0037707	CG16788	RnpS1	56910	10	5
FBgn0037707	CG16788	RnpS1	36580	6	3
FBgn0005649	CG5422	Rox8	v100563	10	5
FBgn0005649	CG5422	Rox8	v41439	12	6
FBgn0011305	CG5655	Rsf1	v22186/TM3	15	10
FBgn0267790	CG9373	rump	42665/CyOtb	6	3
FBgn0039229	CG6995	Saf-B	51759		5
FBgn0265298	CG5442	SC35	v40590	5	3
FBgn0265298	CG5442	SC35	v104978	6	3
FBgn0025571	CG5836	SF1	v13426	3	2
FBgn0040284	CG6987	SF2	v27775/TM3	13	7
FBgn0040284	CG6987	SF2	v27776/TM6B	6	4
FBgn0052423	CG32423	shep	43545	4	3
FBgn0002354	CG1420	Slu7	v103587	5	3
FBgn0262601	CG5352	SmB	v40587	3	2
FBgn0262601	CG5352	SmB	v110713	12	6
FBgn0261933	CG10753	SmD1	v31343/TM6B	8	4
FBgn0261933	CG10753	SmD1	v31342	7	4
FBgn0261789	CG1249	SmD2	v31947	4	2
FBgn0261789	CG1249	SmD2	v31946	8	4
FBgn0261789	CG1249	SmD2	v100690	4	2
FBgn0023167	CG8427	SmD3	v35933	8	5
FBgn0261790	CG18591	SmE	v23569	4	2
FBgn0261790	CG18591	SmE	v23570/TM6B	10	5
FBgn0000426	CG16792	SmF	v107644/CyOtb	lethal	
FBgn0000426	CG16792	SmF	26734	12	6
FBgn0036641	CG16725	Smn	v100392	7	4
FBgn0003449	CG4528	snf	51459	16	8
FBgn0003449	CG4528	snf	55914	9	5
FBgn0016978	CG8749	snRNP-U1-70K	v23150	11	8
FBgn0016978	CG8749	snRNP-U1-70K	v23151	10	6
FBgn0261792	CG5454	snRNP-U1-C	v22132	11	6
FBgn0261792	CG5454	snRNP-U1-C	v22133	10	5
FBgn0261791	CG9742	SNRPG	v39256	10	5
FBgn0015818	CG3780	Spx	v40471	9	5
FBgn0015818	CG3780	Spx	v40472	9	5
FBgn0263396	CG16901	sqd, hrp40	v32395	12	6
FBgn0263396	CG16901	sqd, hrp40	31302	20	10
FBgn0036340	CG11274	SRm160	v6439	9	5
FBgn0036340	CG11274	SRm160	v100751	8	4
FBgn0015298	CG4457	Srp19	51160	lethal	
FBgn0024285	CG4602	Srp54	v51088	8	6
FBgn0024285	CG4602	Srp54	55254	9	5
FBgn0026370	CG8174	SRPK	v103416	9	6
FBgn0025702	CG11489	srpk79D	v47544	8	5
FBgn0025702	CG11489	srpk79D	v47545	10	5
FBgn0003520	CG5753	stau	31247	9	5
FBgn0003559	CG17170	su(f)	v110125	6	3
FBgn0003638	CG3019	su(wa)	v25597	12	9
FBgn0003638	CG3019	su(wa)	v104716	10	5
FBgn0264270	CG43770	Sxl	34393	10	5
FBgn0037371	CG2097	Sym	v33470	9	5
FBgn0038826	CG17838	syp	56972	10	5
FBgn0038826	CG17838	syp	v33012	15	9
FBgn0025790	CG10327	TBPH	v38377	7	4
FBgn0025790	CG10327	TBPH	v38379	10	5
FBgn0003741	CG16724	tra	v2560	12	6
FBgn0003742	CG10128	tra2	v8868	9	5
FBgn0039117	CG10210	tst	v38356	8	4
FBgn0039117	CG10210	tst	v108216	12	6
FBgn0033378	CG8781	tsu	55367	11	6
FBgn0033378	CG8781	tsu	28955	9	5
FBgn0033210	CG1406	U2A	v17358/TM6B	9	5
FBgn0033210	CG1406	U2A	v109815	11	6
FBgn0017457	CG3582	U2af38	v110075	9	5
FBgn0017457	CG3582	U2af38	29304	13	7
FBgn0005411	CG9998	U2af50	v24176	11	6
FBgn0005411	CG9998	U2af50	v24177	10	6
FBgn0036733	CG6322	U4-U6-60K	v34242	8	6
FBgn0036733	CG6322	U4-U6-60K	v110393	10	6
FBgn0030354	CG1559	Upf1	43144	12	7
FBgn0028554	CG10203	xl6	v31203	14	8
FBgn0028555	CG10204	xl6	v100226	11	7
FBgn0021895	CG18426	ytr	55704	4	2